ISBN 978-82-326-3210-7 (printed version)
ISBN 978-82-326-3211-4 (electronic version)
ISSN 1503-8181

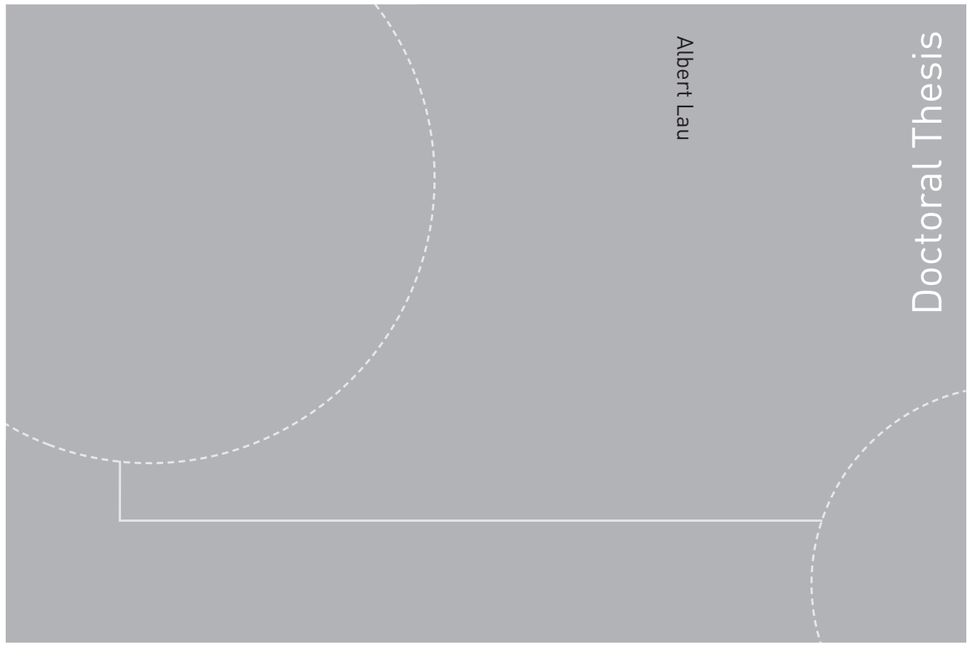

Doctoral theses at NTNU, 2018:210

Albert Lau

Numerical Simulation of Switch and Crossing Towards an Optimized Turnout Design

NTNU
Norwegian University of
Science and Technology
Faculty of Engineering
Department of Civil and Environmental Engineering

NTNU
Norwegian University of
Science and Technology

Doctoral theses at NTNU, 2018:210

NTNU

NTNU
Norwegian University of
Science and Technology

Albert Lau

Numerical Simulation of Switch and Crossing Towards an Optimized Turnout Design

Thesis for the degree of Philosophiae Doctor

Trondheim, June 2018

Norwegian University of Science and Technology
Faculty of Engineering
Department of Civil and Environmental Engineering

NTNU
Norwegian University of
Science and Technology

NTNU
Norwegian University of Science and Technology

Thesis for the degree of Philosophiae Doctor

Faculty of Engineering
Department of Civil and Environmental Engineering

ISBN 978-82-326-3210-7 (printed version)
ISBN 978-82-326-3211-4 (electronic version)
ISSN 1503-8181

Doctoral theses at NTNU, 2018:210

Printed by Skipnes Kommunikasjon as

The committee for the appraisal of this thesis was compromised of the following members:

Associate Professor, Dr. **Guoqing Jing,**
Department of Highway and Railway Engineering,
Beijing Jiaotong University,
Beijing, China.

Senior Engineer, Dr.Ing. **Kjell Arne Skoglund,**
Public Roads Administration,
Trondheim, Norway.

Associate Professor. PhD. **Kelly Pitera,**
Department of Civil and Environmental Engineering,
Norwegian University of Science and Technology,
Trondheim, Norway.

The advisors during the study have been:

Professor, Dr.Ing. **Inge Hoff,**
Department of Civil and Environmental Engineering,
Norwegian University of Science and Technology,
Trondheim, Norway.

Senior Engineer, Dr.Ing. **Alf Helge Løhren,**
Bane NOR,
Trondheim, Norway.

Postdoc, Dr. **Chang Wan,**
Department of Civil and Environmental Engineering,
Norwegian University of Science and Technology,
Trondheim, Norway.

This page is intentionally left blank.

Summary

Switch and crossing (S&C) or turnout is a mechanical component within railway infrastructure that provides flexibility for train to switch from one track to another. However, such flexibility requires certain degree of geometry changes and discontinuities and these changes often result in high impact forces. Because of the high impact forces, damage frequency in turnout is often higher compared to normal track. It often requires more attention compared to normal track too. Therefore, turnout is a very costly component within railway infrastructure.

As a result, researchers have been striving to understand this component better to make it less costly. However, understanding turnout itself is a very costly task especially if the investigations need to be carried out on track on-site. For example, to mount devices on the track, acquiring data and analyzing results are very labor-intensive. In addition, the track needs to be especially made available and special arrangement is needed for the train driver to drive the train over the track under specified controlled conditions. Because of that, many researchers have turned to numerical modelling which is a cheaper alternative.

Multibody simulation (MBS) has been one of the most popular modelling techniques used to model turnout. MBS is well known for its computational efficiency and its capability to model wheel-rail kinematic especially in turnout. However, the tool was originally designed mainly to model train dynamics under train-track interaction. So improvements are still needed when train-track dynamics as a whole is of interested, especially when the role of the track is critical. Therefore, in this study, two improvements have been made in turnout modelling in MBS with an aid of a commercially available MBS software, GENSYS.

The first improvement is to include yaw effect of train's wheelset during the simulation. Conventionally, the wheelset of a train is assumed to be always perpendicular to the track axis during the simulation. However, when a train is travelling through curves, especially small curves, the wheelsets often inherit certain level of angle of attack. This applies in turnout too because of the absence of the cant elevation in turnout. Thus, a methodology has been developed to include the yaw effect of the wheelsets in the simulation. It is concluded that the yaw effect has influence towards contact point calculation and eventually train derailment prediction.

The second improvement is development of a better track modelling approach in the MBS environment. Conventionally, the track in MBS is modelled as a lumped mass following the train wheels during the simulation. This type of track model is sufficient for normal railway track modelling. However, for turnouts of which bending stiffness of the rail and geometry of the sleeper changes immensely along the track, lumped mass track assumption is no longer sufficient. Therefore, an approach considering full track model in the simulation that is fixed in the continuum includes rails discretely supported by sleepers sitting on an elastic foundation has been developed. The train travel through the track instead of having the track follows the train during the simulation. With this track, some important parameters such as rail bending stiffness variation and sleeper geometry variation have been made possible to

be included in the modelling. Besides, time history of the track such as force exerted on the sleepers, sleeper displacement, and force exerted on the ballast have been made possible to be studied. Based on the development, a right hand 60EI-R760-1:15 turnout without rail inclination has been modelled. The effect of the rail bending stiffness variation and sleeper geometry variation has been discussed.

Finally, the turnout model is used for an optimization task. The aim of the optimization task is to find the optimized railpad stiffness for the turnout by using an optimization technique call genetic algorithm. Different cases such as two different train types, different ballast stiffness and travelling directions have been considered. A guideline for the best railpad vertical stiffness of the turnout under a specific setup has been suggested by the optimization. In conclusion, soft railpad stiffness is recommended as long as vertical compressive displacement of the railpad does not exceed 2 mm. Besides, it might be safe to use railpad with vertical stiffness of 33 MN/m throughout the turnout as long as the axle load of the train is not more than 22.5 ton and the train is not travelling faster than 200 km/h.

Keywords: Switch and crossing, turnout, wheelset yaw, Full MBS track, railpad optimization

Contents

Summary iii
Contents v
Preface vii
List of figures ix
List of appended papers xi
1. Introduction 1
1.1 Background and motivation 1
1.2 Objective 3
1.3 Scope 4
1.4 Thesis outline 4
2. Numerical train-track model 5
2.1 Train modelling 5
2.2 Track modelling 6
2.3 Turnout modelling 9
2.3 Train-track coupling 10
2.4 Modelling results 13
3. Numerical train-turnout optimization 19
3.1 Train-turnout model simulation improvement 20
3.2 Optimization process 22
3.3 Optimization results 25
4. Conclusion 27
5. Future work 29
Reference 30

This page is intentionally left blank.

Preface

The work presented in this thesis was carried out at the Department of Civil and Environmental Engineering, Norwegian University of Science and Technology in Trondheim between October 2014 and March 2018.

Needless to say, this thesis would not be possible without the supports from many. I would like to thank Jernabanedirektoratet for financing my position as a PhD candidate. I would also like to thank Prof. Elias Kassa for opening this opportunity to me.

To my very caring and competent supervisors Prof. Inge Hoff, Dr. Alf Helge Løhren and Dr. Chang Wan. Thank you for guiding me through this PhD. Thank you Dr. Chang Wan for encouraging me to apply for this position. During my toughest part of my PhD, all of you did not lose faith in me but provided me the very much-needed trust has been the key for me to find the breakthrough. Your professional effort and dedication are highly appreciated and will be remembered for the rest of my life.

To Prof. Xiaopei Cai, thank you for your generous guidance and advices especially during the beginning stage of my PhD. It has been very crucial for the development of this thesis.

To Mr. Ingemar Persson, thank you for your advices and guidance in modelling in GENSYS.

To Dr. Alejandro De Miguel Tejada, Prof. Ilmar Santos and Mr. René Fongemie, thank you for the very fruitful collaboration and inviting me to spend 3 months in DTU. Many ideas and inspirations for the development of this thesis were found through this collaboration.

To my colleagues both in NTNU and in Bane NOR, thank you for providing me such a pleasant working environment. Special thanks to Dr. Sara Anastasio, Dr. Petr Pokorny, Ms. María Díez Gutiérrez, Mr. Gunnstein Frøseth and Prof. Anders Rønnquist for the very much-needed supports during the toughest period of my PhD.

To Dr. Carl Thodesen for your kind help during the transition period of my PhD.

To my friends in Malaysia especially Mr. John Tiong, Ms. Yvonne Yong, Mr. Koh Jing Han and Ms. Choot Sin Ling. It is your faith in me that enabled me to pursue this career.

Last but not least, to my family, thank you for the support all this while especially to the most important person in my life, Eileen Lau for always being by my side, I love you.

Trondheim, April 2018

Albert Lau

This page is intentionally left blank.

List of figures

Figure 1-a: Switch and crossing 1
Figure 1-b: Moving mass track model 2
Figure 1-c: Wheel position in simulation vs. reality 3
Figure 1-d: Thesis outline 4
Figure 2-a: Schematic train-track model 5
Figure 2-b: Eigenvalues and eigenmodes of the train 6
Figure 2-c: Full track model 7
Figure 2-d: Track model comparison 8
Figure 2-e: Eigenvalues and eigenmodes of the track 8
Figure 2-f: Rail sectional profiles in diverging move [15] 9
Figure 2-g: Aerial view of the train-turnout model 10
Figure 2-h: Traditional contact calculation 11
Figure 2-i: New contact calculation including yaw effect of the wheelset 12
Figure 2-j: Traditional contact calculation (noyaw) vs. new contact calculation (yaw) 13
Figure 2-k: Vertical normal force of the wheels on the leading wheelset 14
Figure 2-l: Sleeper passing effect 15
Figure 2-m: Force exerted on the sleeper 16
Figure 2-n: Maximum force exerted on the ballast 17
Figure 3-a: Railpads 19
Figure 3-b: Transient effect removal 21
Figure 3-c: Zone definition 22
Figure 3-d: MATLB - GENSYS communicating process 24
Figure 3-e: Vertical wheel force in diverging direction 25
Figure 3-f: Force exerted on the sleeper under the left rail in diverging direction 26

This page is intentionally left blank.

List of appended papers

This thesis consists of a summary of the present work and a collection of the following appended papers:

Paper A

A. Lau and E. Kassa, *'Simulation of vehicle-track interaction in small radius curves and switches and crossings'*, Proceedings of the Third International Conference on Railway Technology: Research, Development and Maintenance, Cagliari, 2016.

Lau initiated the study, performed the simulations, analyzed the results and wrote the paper. Kassa contributed with advices for development of the methodology, planning of the paper, and for the simulation throughout the process.

Paper B

A. Lau and I. Hoff, *'Simulation of train-turnout coupled dynamics using a multibody simulation software'*, manuscript is under review in Modelling and Simulation in Engineering by Hindawi, 2017.

Lau initiated the study, performed the simulations, analyzed the results and wrote the paper. Hoff contributed with advice throughout the process and comments to the text.

Paper C

A. Lau, C. Wan, A. H. Løhren and I. Hoff, *'A methodology for switch and crossing optimization'*, Accepted for publication in American Society of Civil Engineers (ASCE).

Lau initiated the study, performed the simulations, analyzed the results and wrote the paper. Wan, Løhren and Hoff contributed with advice throughout the process and comments to the text.

Paper D

A. Lau, C. Wan, A. H. Løhren and I. Hoff, *'Numerical switch and crossing railpad vertical stiffness optimization'*.

Lau initiated the study, performed the simulations, analyzed the results and wrote the paper. Wan, Løhren and Hoff contributed with advice throughout the process and comments to the text.

Papers not included in this thesis

X. Cai, L. Zhao, **A. Lau**, S. Tan and R. Cui, *'Analysis of vehicle dynamic behavior under ballasted track irregularities in high-speed railway'*, Noise and Vibration Worldwide, Vol 46, Issue 10, pp. 10-17.

A. M. Tejada, **A. Lau**, I. F. Santos and R. Fongemie, *'Numerical simulation of track settlement using a multibody dynamic software – A holistic approach'*, Proceedings of the XVII International Symposium on Dynamic Problems of Mechanics (DINAME 2017), Sao Paolo, 2017.

A. M. Tejada, **A. Lau**, and I. F. Santos**,** *'Numerical simulation of track settlements based on an iterative holistic approach',* manuscript is under review in Journal of the Brazilian Society of Mechanical Sciences and Engineering, 2018.

A. M. Tejada, F. Jacobsen, **A. Lau**, and I. F. Santos, *'Uncertainty analysis of track degradation at railway turnouts aided by a multi-body simulation software'*, manuscript has been accepted for publication in Part F: Journal of Rail and Rapid Transit, 2018.

1. Introduction

1.1 Background and motivation

Switch and crossing (S&C) or turnout as illustrated in figure 1-a is a mechanical component that provides the flexibility to railway trains to switch from one track to another. Switchblade in switch panel can be moved laterally into one of two positions to lead the train into through route or diverging route. Whereas crossing is a component that distinguishes through and diverging route.

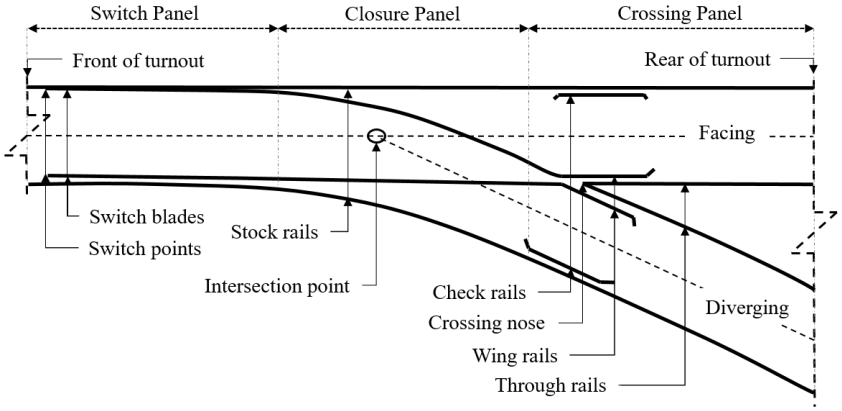

Figure 1-a: Switch and crossing

However, such flexibility requires certain degree of geometry changes and discontinuities in both switch panel and crossing panel. Because of the geometry changes and the discontinuities, high impact forces can often be observed within turnout. The high impact forces is also the main contributor to the damage of the component and highly in need for attention i.e. maintenance and renewal. Therefore, sometimes turnout is regarded as 'hungry asset' in railway infrastructure.

Based on the database in Bane NOR (Norwegian National Rail Administration), there are 3548 turnouts in 4475 km Norwegian railway network for both network in regular and non-regular operation, of which the turnouts consist of approximately 3.1 % of the total Norwegian railway network length. However, in 2015, approximately 35 % of the entire cost of maintenance of the superstructure was spent on turnout related faults [1]. In addition, 55 % of the faults recorded in 2015 were turnout related [2].

As a result, researchers have been striving to understand turnout better to make it less costly. However, understanding turnout itself is a very costly task especially if the investigations need to be carried out on track on-site. For example, to mount devices on the track, acquiring data and analyzing results are very labor-intensive tasks. In addition, the track needs to be specially made available and special arrangement is needed for the train driver to drive the train over the track under specified controlled conditions. Because of that, many researchers have turned to numerical modelling which is a more economical alternative.

Two types of numerical methods are commonly used in the simulation of train or/and track dynamics i.e. multibody simulation (MBS) method and finite element method (FEM). MBS is efficient to study train-track dynamics but the trade-off is that the track has to be simplified. In FEM, a very detailed train-track model can be modelled including bodies' structural flexibility; however, the computational effort is usually very high. Therefore, FEM in railway field has often been used for very detailed component modelling [3], detailed wheel-rail contact modelling [4, 5]. Sometimes FEM is also used for train-track simulation as a whole, but simplifications are often necessary to reduce the computational effort [6, 7].

MBS is preferable when it comes to study train-turnout interaction as a whole. MBS tools dedicated for train-turnout interaction analysis are well known for having a wheel-rail contact module that is able to model complex wheel-rail kinematic behaviour and to calculate the creep forces. Some authors, for example Kassa et al. [8], Lagos et al. [9], Wan et al. [10], Pålsson [11], and Lau et al. [12] used MBS to simulate train-turnout dynamic interaction to evaluate the maximum contact forces along a railway turnout, to study dynamic effects of different wheel profiles running through different turnout designs, to optimize crossing nose geometry, to optimize switch geometry and to study the effect of wheelset yaw in a turnout.

However, the track in the train-turnout model used by the abovementioned authors are mass moving model represented by a lumped mass or mass layers coupled using series of springs and dampers, see figure 1-b. The track follows the train's wheels throughout the simulation. Such track model is able to capture dynamics up to 200Hz but some frequencies such as sleeper passing frequency and frequencies induced by the rail bending stiffness cannot be modelled. Moreover, constant sleeper mass is used in the model. The constant sleeper mass is not a problem for a nominal track modelling; however, in turnout, this assumption is no longer hold valid. In addition, the wheelset in the model is assumed to be always orthogonal to the track axis. However, due to the absence of cant elevation and sometimes rail inclination in turnout, the wheelset often travels with large angle of attack especially at the entrance of a curve or a turnout see figure 1-c.

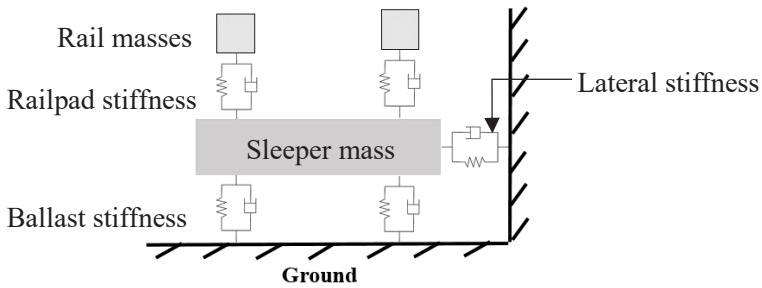

Figure 1-b: Moving mass track model

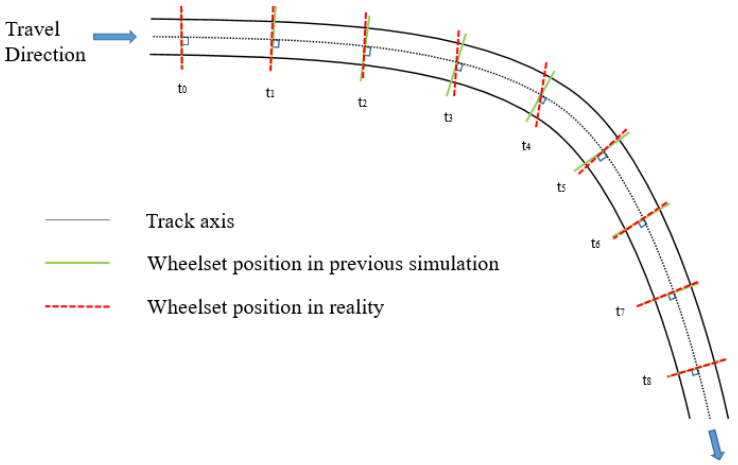

Figure 1-c: Wheel position in simulation vs. reality

In this study, an improved train-track model has been developed with an aid of a commercially available Multibody simulation software GENSYS [13]. Two major improvements have been achieved in the model. The first improvement is the yaw angle of the wheelset can be accounted for during simulation. This allows wheel-rail contact information to be predicted more accurately. The second improvement is development of a better track modelling approach. Through this approach, the track in the train-track model is able to account for rail bending stiffness and varying it element-wise. Moreover, sleeper geometry properties such as mass, dimension, and moment of inertia can be varied in the track. This approach makes prediction of track information such as time history of the sleeper, force exerted on the sleeper and force exerted on the ballast possible. Through this approach, a right hand turn 60EI-R760-1:15 (Standard UIC 60kg/m rail, radius 760 m, 1 in 15 crossing angle) turnout, also called full train-turnout model has been modelled. The improved model and its capabilities have been discussed in chapter 2.

With the improved full train-turnout model, an attempt has also been made to optimize its railpad vertical stiffness using an optimization technique namely genetic algorithm. A general guideline of the optimized railpad vertical stiffness according to a specific setup in the turnout has been suggested by the optimization. The optimization setup and results have been discussed in chapter 3.

1.2 Objective

The objectives of this work are:

1. Develop a better train-turnout coupled numerical model and after that,
2. Utilize the model to numerically optimize turnout's design.

1.3 Scope

The overall scope of this thesis are summarized as below:

1. Integrate yaw effect of wheelset into numerical modelling.
2. Develop a better track model especially to simulate train-turnout dynamics.
3. Utilizing the model to optimize vertical stiffness of the railpad in a specific turnout.

1.4 Thesis outline

The thesis outline is illustrated in figure 1-d:

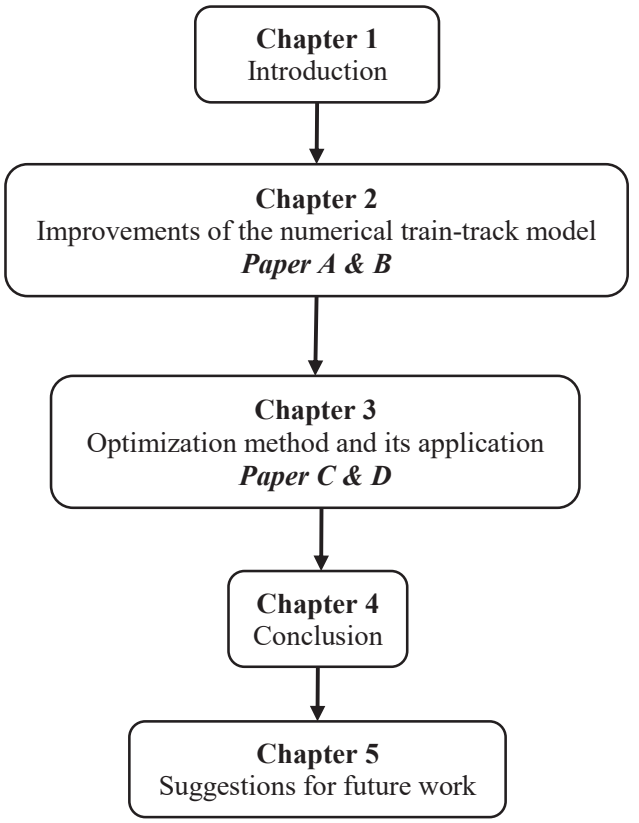

Figure 1-d: Thesis outline

2. Numerical train-track model

All the numerical train-track models modelled in this study are achieved by using a commercially available multibody simulation (MBS) software GENSYS. Two mathematic programming platforms namely MATLAB and OCTAVE have been used for post-processing the results.

2.1 Train modelling

Two types of trains have been used in this study namely passenger train (Norwegian Flirt Train) and freight train (train with Y25 bogies). Both the train models consist of seven bodies i.e. one carbody, two bogies and four wheelsets as illustrated in figure 2-a. The carbody and the bogies have six degrees of freedom (DOF), three translations and three rotations. The wheelsets have five DOFs with the longitudinal displacement being constrained. The bodies are coupled using series of springs and dampers representing the suspensions of the train.

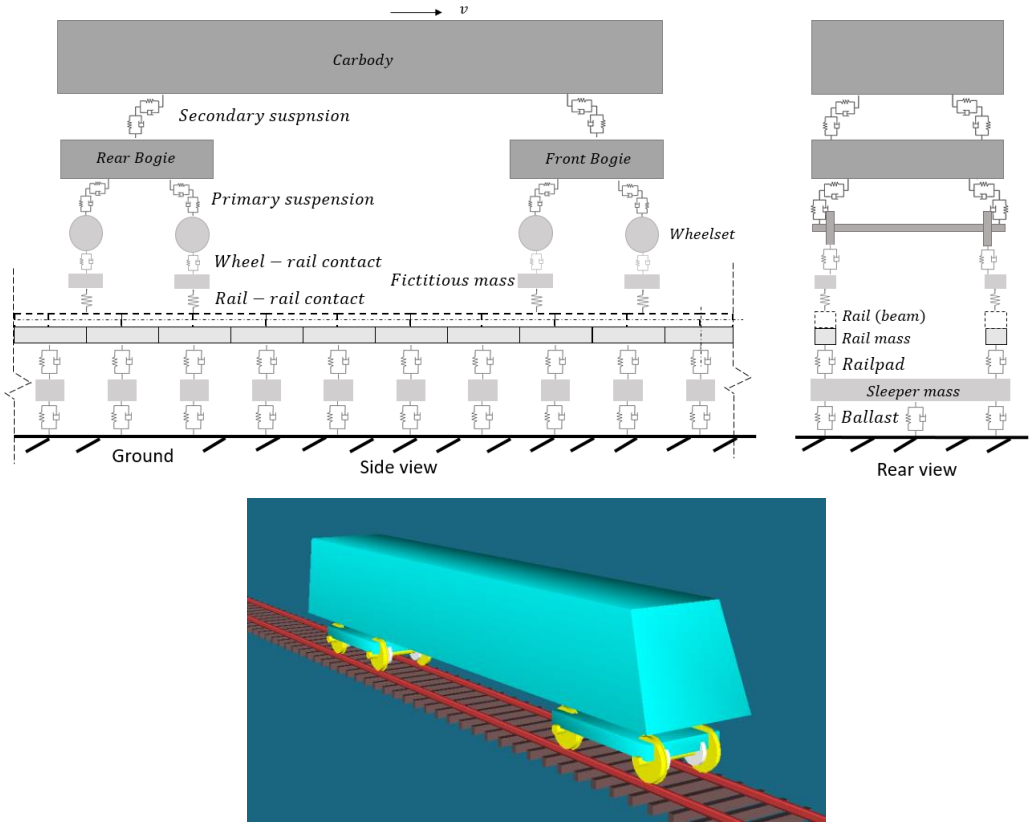

Figure 2-a: Schematic train-track model

The major differences between the trains are the weight of the train and the suspensions properties of the trains. The axle load of the passenger train and the freight train are 19 ton and 22.5 ton respectively. To ensure the trains behave as close as possible to reality, they have been calibrated (without track) via modal analysis with good match on eigenvalues and eigenmodes compared to the ones provided by the manufacturers. Some of the principal eigenvalues and eigenmodes of the passenger train are illustrated in figure 2-b.

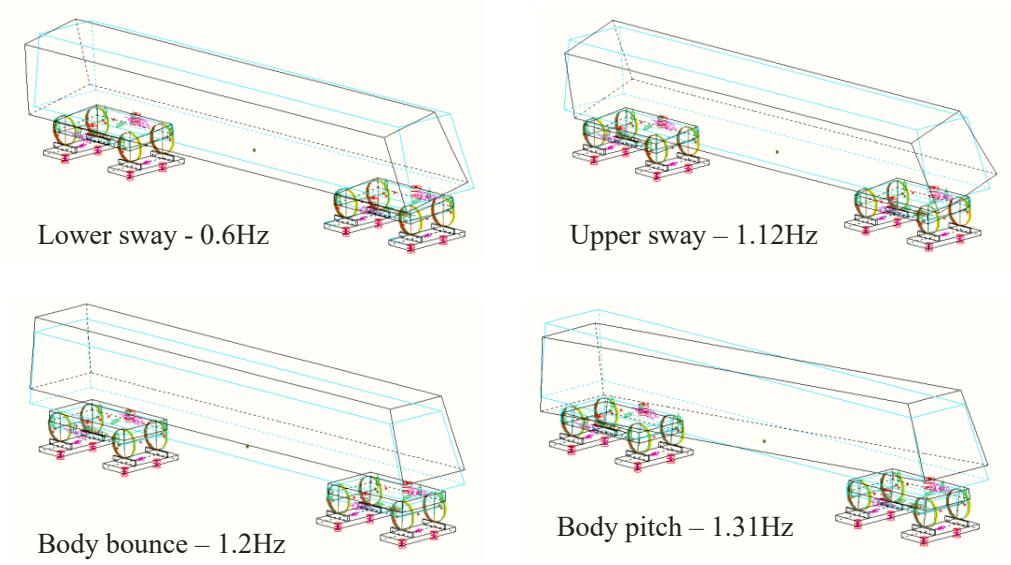

Figure 2-b: Eigenvalues and eigenmodes of the train

2.2 Track modelling

As mentioned earlier, conventionally, the track used in MBS is quite simple, a moving lumped mass track model. This kind of track is not an issue for nominal track as the rail bending stiffness and sleeper is more or less always constant. However, this assumption is no longer sufficient when it comes to railway track component such as turnout of which the rail bending stiffness and the sleeper geometry are not the same along the turnout. In addition, lacking of time history of the track is a problem especially if the track dynamics is of interest. Thus, a better track modelling approach has been specifically developed to address these problems.

Through this modelling approach, railway track can be modelled as a full track model (figure 2-c) instead of just a lumped mass in addition to the train model. The rail in the full track model is modelled using Euler-Bernoulli beam theory. The beam is modelled element-wise with Dirac delta function and unit step function in order to make altering bending stiffness of the beam possible yet exhibits support condition effect of the track. More masses and stiffness can also be coupled under the beam to mimic other track components such as

sleepers and ballast stiffness. By modelling a full track model using this approach, the time history of the track component behaviour such as rail bending moment, force exerted on the sleepers, sleeper displacement and force exerted on the ballast can be studied. This feature makes investigation of the track related tasks possible. For example, track component optimization, track settlement prediction, component acceleration analysis, etc. However, the downside of this approach is that the bending stiffness can only be altered element-wise which is at every sleeper support distance. Figure 2-d illustrates a comparison between a bogie travelling on a full track and on a moving mass track.

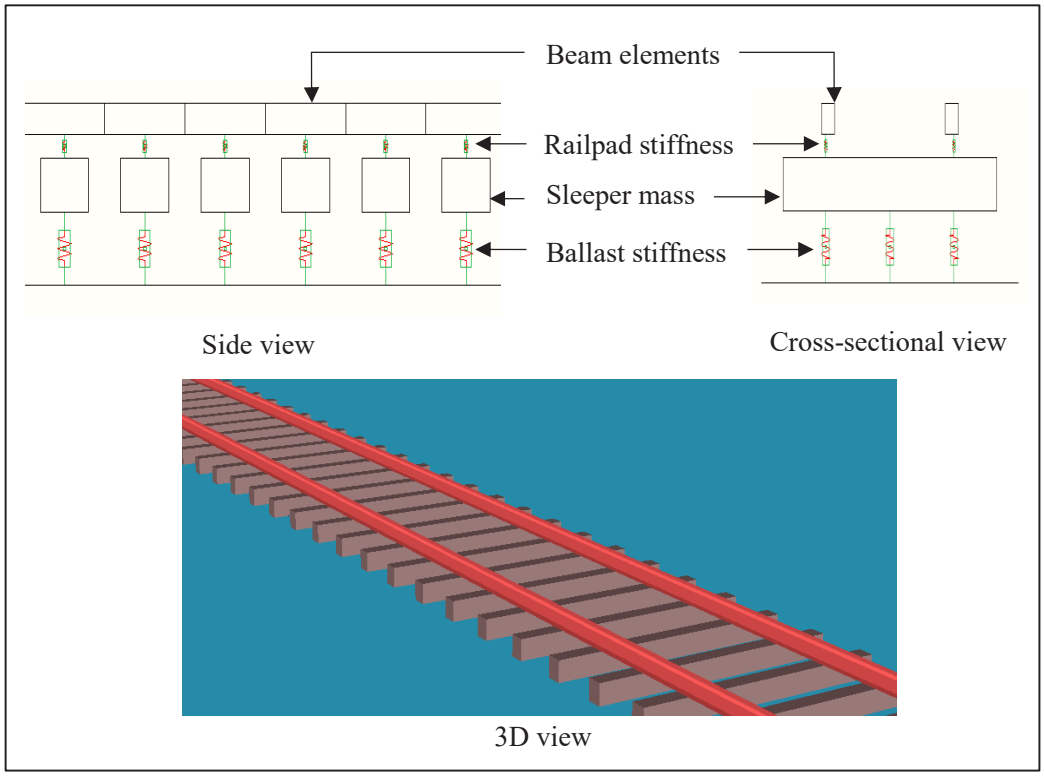

Figure 2-c: Full track model

As a validation purpose, first, a 30 m straight track has been modelled using this approach. The validation has been performed using a numerical receptance test. The scope of the validation involves tuning track parameters such as railpads and ballast stiffness and compared the corresponding receptance test results to the one that has been validated and recorded in a literature [14]. With that, track properties that allow the track to work realistically have been obtained. The track properties can be found in table 1 in ***Paper B.*** These track properties are also used in the full turnout model later.

Similar to the train model, a modal analysis has been performed on the track (without train). The three principal eigenvalues and eigenmodes can be observed in figure 2-e. It is also

observed that the eigenvalues are very similar to the resonance frequencies found in the receptance test even though the track model has been linearized in the modal analysis.

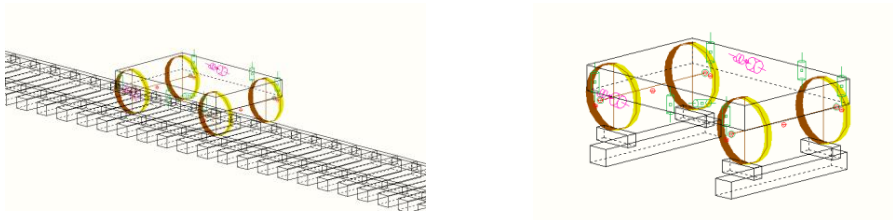

Figure 2-d: Track model comparison

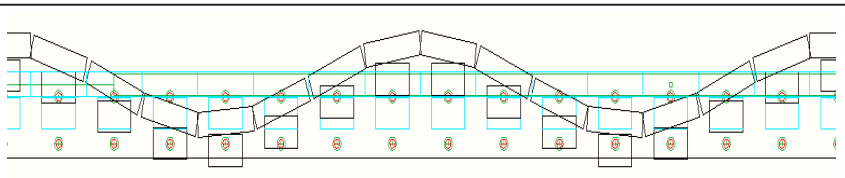
(1) Rails and sleepers bouncing on the ballast – 129.10 Hz

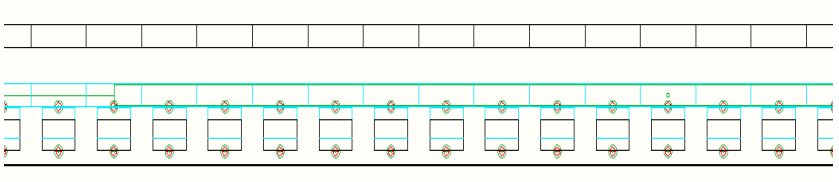
(2) Rails bouncing on the sleepers – 505.08 Hz

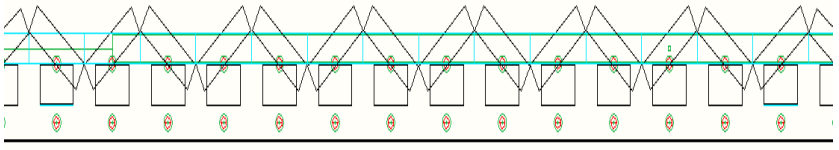
(3) Pin-pin resonance – 830.48 Hz

Figure 2-e: Eigenvalues and eigenmodes of the track

2.3 Turnout modelling

A turnout model has been modelled using the developed approach. The turnout considered in this study has been a right hand 60EI-R760-1:15 turnout without rail inclination. The turnout model has three major differences compared to the nominal track:

1. 30 different rail profiles are used in the turnout model to account for the rail profile variation in the turnout, see figure 2-f. Obtaining the rail profiles is a very tedious task. This requires a special device call Miniprof for turnout to measure the cross-sectional profiles at very short interval along the turnout. Since the Miniprof for turnout device is not available in Norway, the profiles used in this study has been the profiles measured earlier in Sweden and they come together with GENSYS. This is also the reason only one turnout has been used in this study. Because of the profile variation, a special algorithm developed by Kassa et al. [15] is needed when it comes to contact information calculation.
2. The rail bending stiffness is varied element-wise in switch and crossing panels along the turnout. The bending stiffness information can be found in Appendix 1 in ***Paper C***.
3. The sleepers' mass, dimension and moment of inertia are varied according the real turnout sleeper construction in the turnout model.

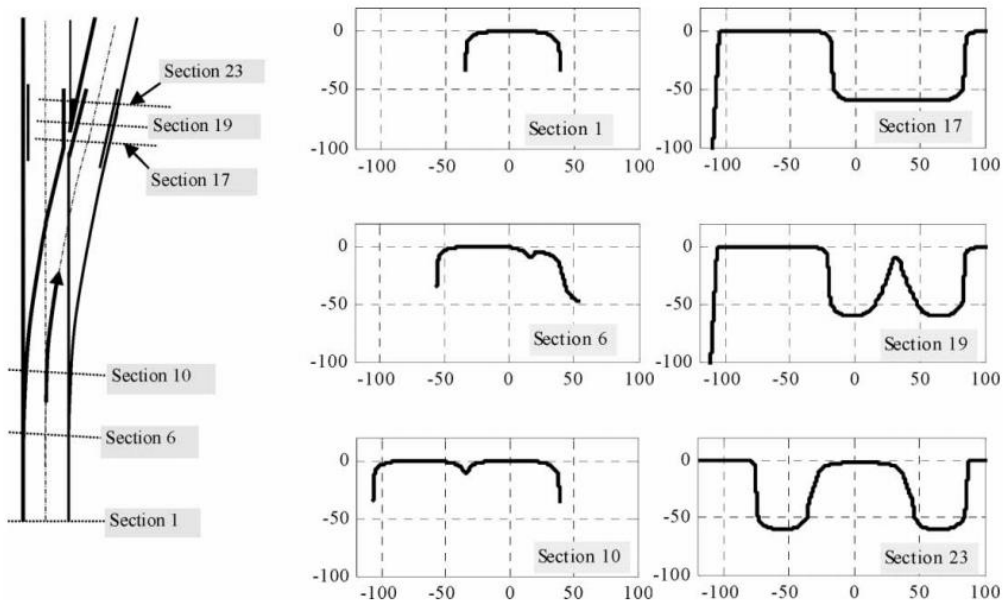

Figure 2-f: Rail sectional profiles in diverging move [15]

The total length of the full turnout model in MBS is 120 m, 60 m of straight track modelled to damp the initial transient effect, followed by 60 m of the turnout. Therefore, the model consists of 400 rail masses, 200 sleeper masses and 1000 spring-damper elements (railpads and ballast of the track). The railpad and ballast stiffness and damping follow the validated

track properties that were validated from a 30 m straight track model as mentioned in section 2.2. The sleeper span of the turnout model is set as 0.6 m. Figure 2-g shows the passenger train travelling through the turnout in the facing direction.

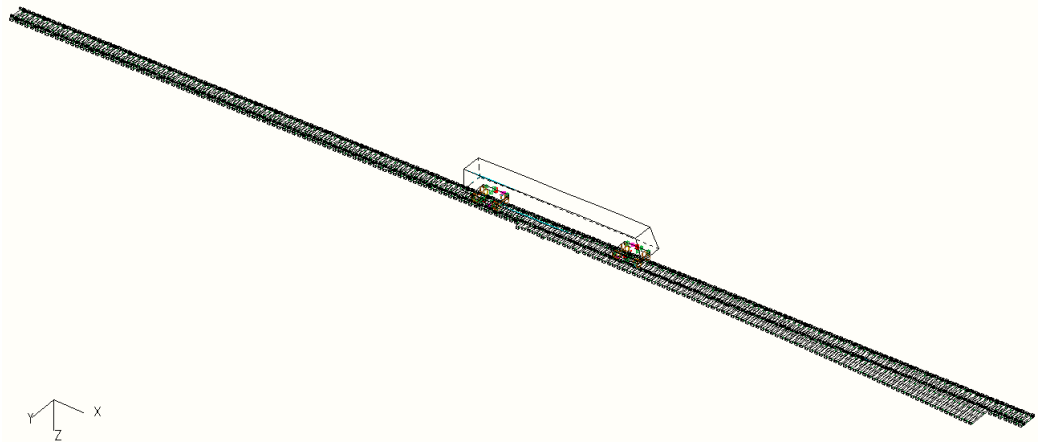

Figure 2-g: Aerial view of the train-turnout model

2.3 Train-track coupling

For coupling of the train and the track (figure 2-a), a stiff series of spring and damper (k=141MN/m, c= 30kNs/m) is used under each wheel connect to a neglected inertia fictitious mass. The fictitious masses are required in order to extract wheel-rail profile contact information and track irregularity (if any) during the time simulation. The contact information are pre-calculated and saved in a lookup-table. The fictitious masses are then connected to the rails (beam element) by a stiff 'rail-rail' contact stiffness, which has a value of 5000 MN/m, assuming the wheel and the rail do not lose contact during the simulation. For normal wheel-rail contact problem, Hertz contact theory is adopted. Creepages and creep forces are solved by using the FASTSIM algorithm.

However, there is a downside of the pre-calculated lookup-table method which is the contact information are calculated assuming the wheelset is always orthogonal the track axis, see figure 1-c. This assumption is more or less true if the wheelset is traveling on a straight track. However, the assumption is no longer hold valid for the case when the wheelset is traveling through a tight curve. This is because the wheelset often experiences insufficient creep forces for a perfect steering. Therefore, the wheelset often exhibits a large angle of attack especially at the entrance of a tight curve in order to achieve rolling radius difference equilibrium to steer the wheelset into perfect tangent position. This phenomenon is also very common in turnout because of the absence of the cant elevation.

Since the interaction of the train and the track relies mainly on a small contact area between the wheel and the rail, excluding the yaw effect might have certain effect towards the

estimation of the contact calculation. Therefore, one of the tasks in this study is to include the yaw effect of the wheelset into the simulation (***Paper A***).

Originally, the contact information i.e. wheel-rail rolling angle, contact position, contact area, etc. are calculated using a contact point function module in GENSYS based on the 2D wheel profile displaced laterally relative to the 2D rail profile within a certain defined range. So during the train-track time simulation, the contact information are obtained only by referring to the lateral position of the wheelset for each time step. The procedure is briefly illustrated in figure 2-h.

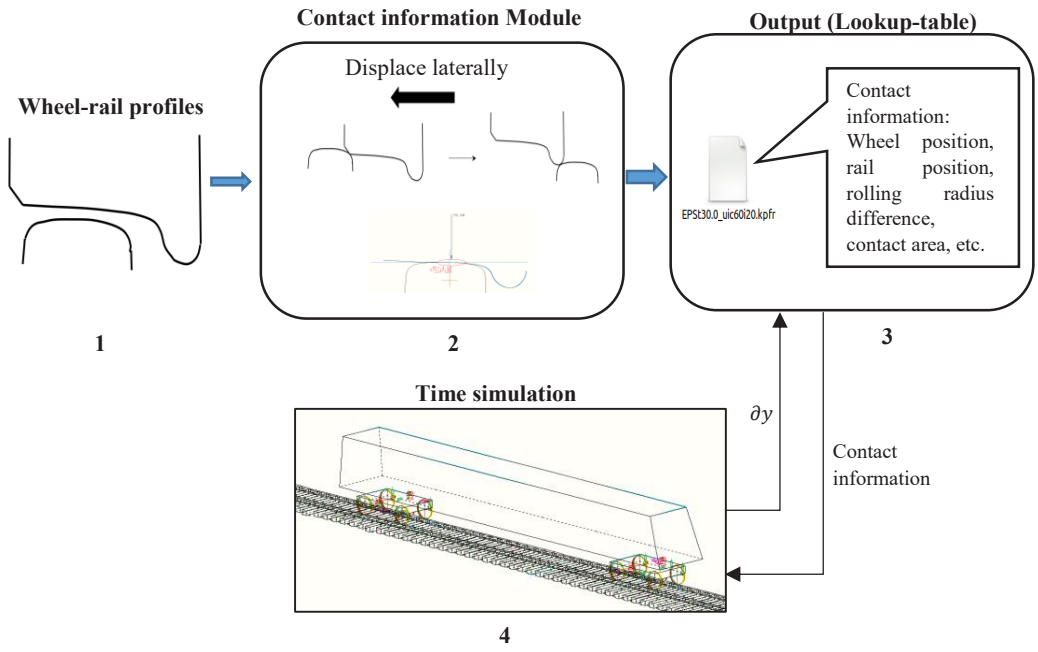

Figure 2-h: Traditional contact calculation

The concept of integrating the yaw effect of the wheelset is very similar to the original methodology and is also achieved via offline lookup-table method with some extra steps. The sequence of the steps are as below. This is also illustrated in figure 2-i.

1. Providing the contact point function module with 2D wheel and rail profiles.
2. The wheel profile is yawed by 2D transformation with maximum and minimum allowable yaw angles. Depending on the fineness of the calculation, the interval of the yaw angle can be adjusted. In this case, only three profiles are considered namely original, maximum and minimum yaw angles. The maximum and minimum yaw angles are when the wheel flange of the wheelset is in contact with the rail.
3. Contact information for all the three profiles are calculated using the contact calculation function module.

4. The outputs generated from the contact information calculation at this stage are still unprocessed.
5. When the wheelset is yawed with a positive angle of attack, the flange contact occurs slightly quicker when the wheelset is displaced laterally. To account for this effect, a contact point information merging process has to be done. Essentially, the merging process is just removing a short section of the wheel profile between thread contact and flange contact. A new processed contact point information result is generated.
6. During the time simulation, the contact information are obtained by referring to both lateral position of the wheelset and the yaw angle of the wheelset.

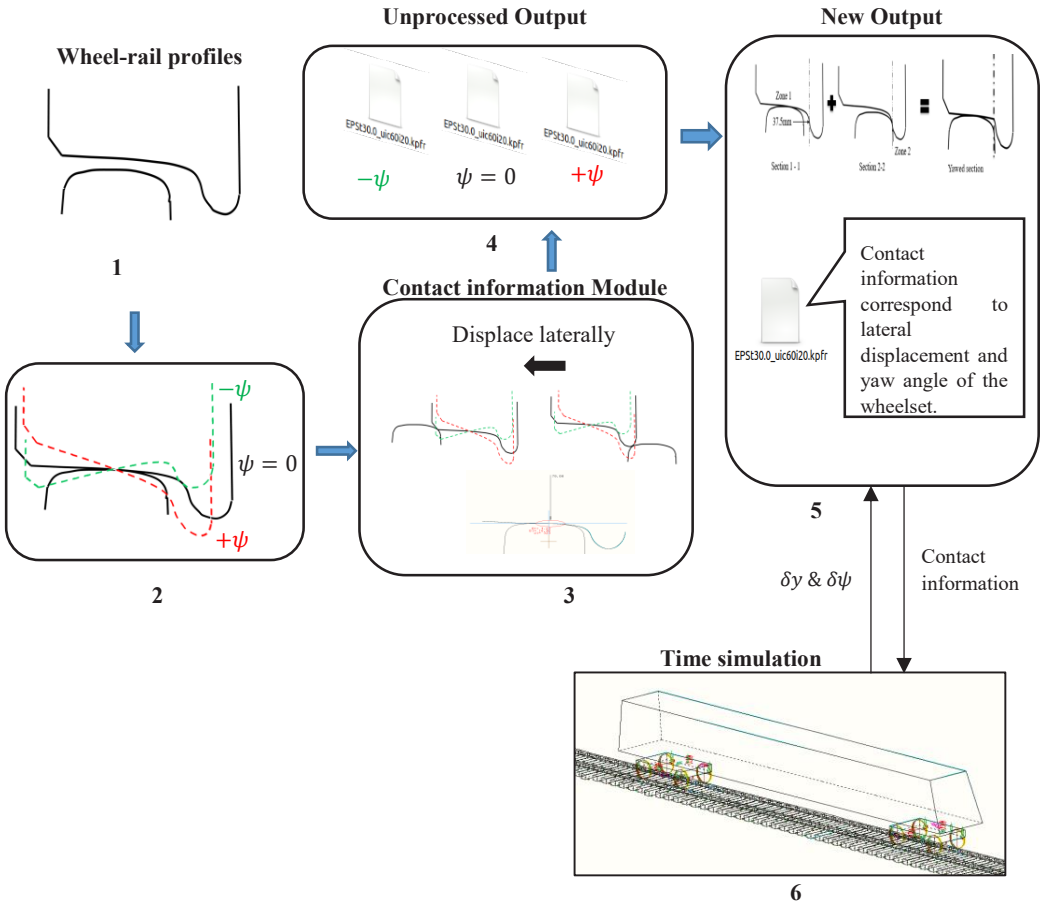

Figure 2-i: New contact calculation including yaw effect of the wheelset

2.4 Modelling results

All the improved modelling results can be found in ***Paper A*** and ***Paper B***. However, for the completeness of this chapter, some of the key results have also been included.

The first result is the behavior of wheel-rail contact when yaw effect is included in the modelling compared to when the yaw is neglected, see figure 2-j. In this case, the freight train is travelling through the 60EI-R760-1:15 turnout (only the switch part). The track model used in this simulation is a moving mass model. The turnout starts at the distance of from 30 m to 90 m. It can be seen that the yaw angle of the wheelset has some effect towards the wheelset yaw, lateral displacement of the wheelset and contact point location on the wheels especially at the entrance of the switch panel. However, the effect is not very significant because of the large turnout radius. The effect will be higher as the curve radius gets lower.

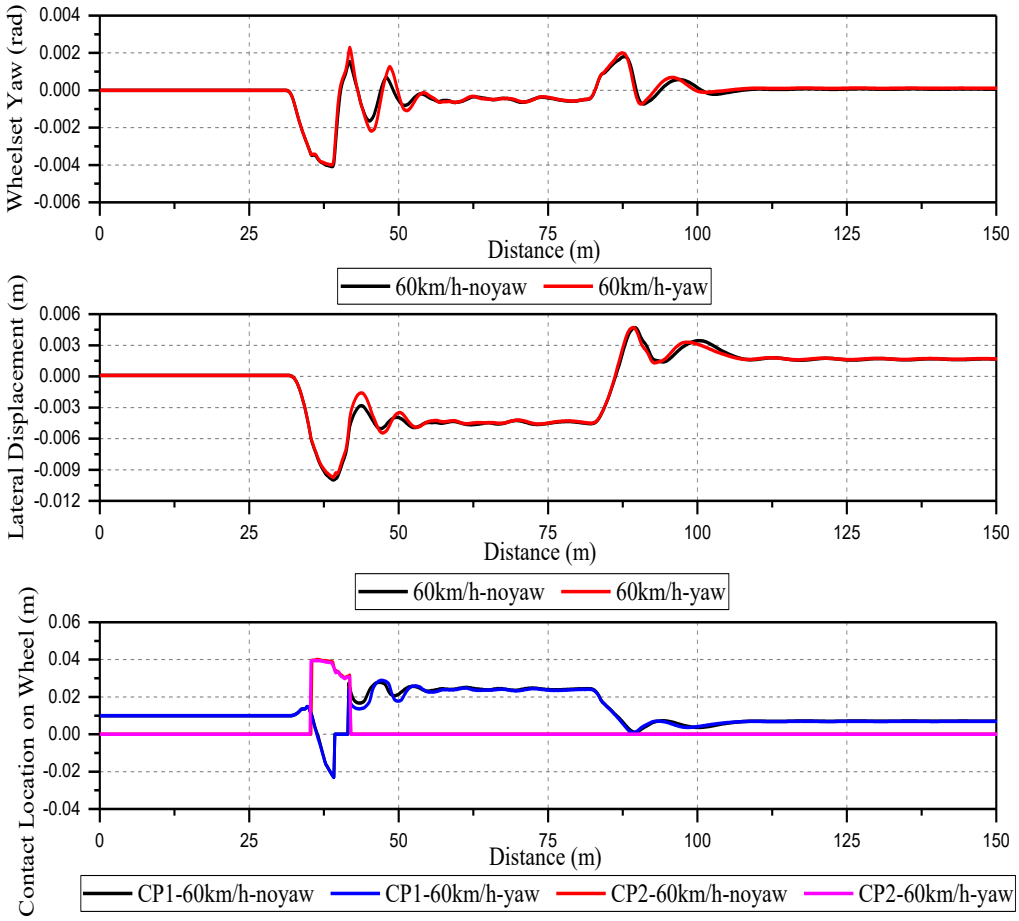

Figure 2-j: Traditional contact calculation (noyaw) vs. new contact calculation (yaw)

The second result is the unfiltered vertical normal force of the wheels on the leading wheelset for the full turnout model compared to moving mass turnout model, see figure 2-k. It can be seen that the vertical normal force are very similar in general for the both models. However, some variation can be observed especially in switch and crossing panels where the dynamic impact is higher. This is probably because of the rail bending stiffness variation effect and the track reacted to the dynamic impact differently compared to the moving mass model and eventually affects the magnitude of the vertical normal force. Nevertheless, the overall results of the full turnout are in good agreement with the widely accepted conventional mass moving train-turnout model. This verifies the validity of the results obtained from the full turnout model. Figure 2-l shows the zoomed in vertical normal force of the wheel. Sleeper passing effect as mentioned earlier can also be simulated in the full turnout model but not in the moving mass turnout model.

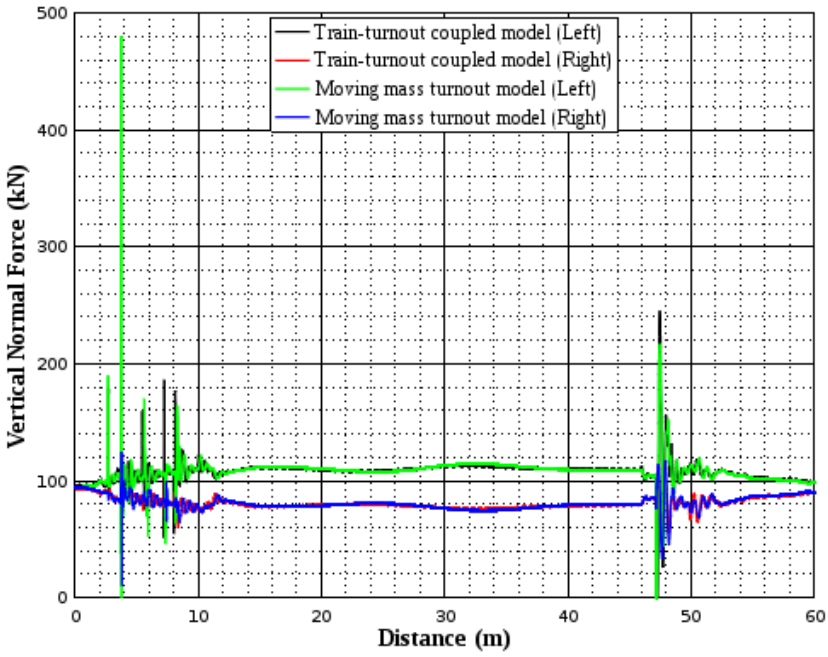

Figure 2-k: Vertical normal force of the wheels on the leading wheelset

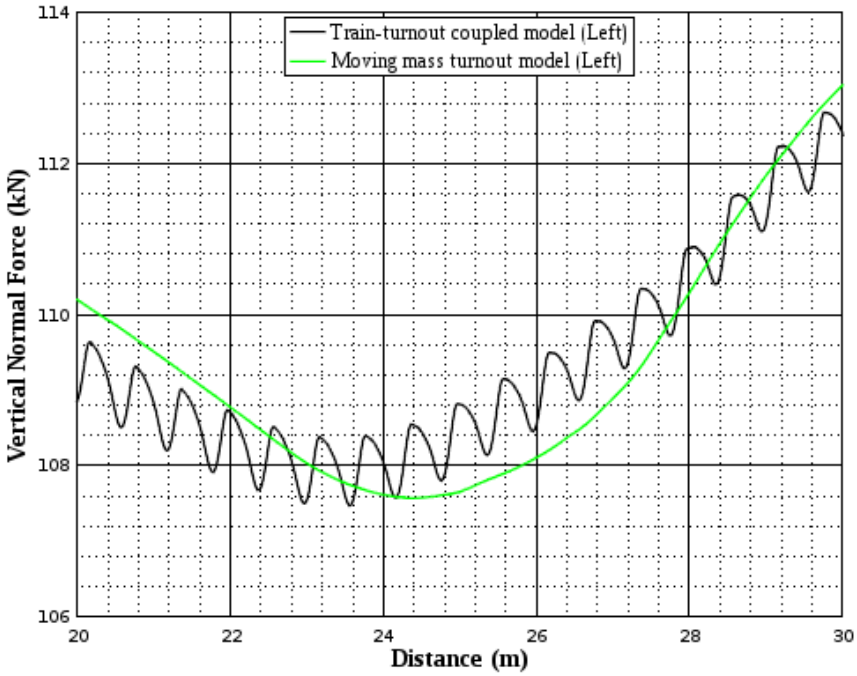

Figure 2-l: Sleeper passing effect

The third result is the force exerted on the sleepers. This result can only be observed in the full track but not in the moving mass track. Figure 2-m illustrates the forces from the left and the right rail exerted on the sleeper number 2, 40, and 80 near the switch panel, closure panel and crossing panel respectively. All the four wheel passages can be observed in the sleeper number 2 and number 40. However, only the first two wheel passages can be observed at the sleeper number 80 due to the length of the track and the trailing bogie did not travel through it before the end of the simulation. It can be seen that the distribution of the forces is even for the first two wheel passages on the sleeper number 2 but the force gradually distributed more to the left wheel when the rear wheels passed the sleeper because of the curvature experienced by the train. The curvature effect becomes more obvious at the sleeper number 40. In addition to the curvature effect, the dynamic impact due to the crossing profile in the sleeper number 80 can be observed.

The last result in this section is the maximum force exerted on the ballast, see figure 2-n. The ballast in the model is modelled as series of spring-damper elements coupling the sleepers to the ground on three different spots left, middle and right. The maximum force exerted on the ballast on the left, middle and right started at around the same magnitude 30kN. Due to the sleeper formation of the turnout as mentioned earlier, the maximum force exerted on the ballast on the right increases gradually and vice versa for the left. However, the maximum force exerted on the ballast in the middle does not fluctuate as much as the left and the right. Coincidently, at the sleeper number 13, the maximum force exerted on

the ballast for all three points are very similar because of the balance of curvature and turnout geometry effect. In addition, due to the change of the sleeper geometry back to the ordinary geometry started from sleeper number 93, a reversal effect of the left and the right maximum force exerted on the ballast due to the carbody roll can also be observed. This highlights the importance of modelling the sleeper variation in the turnout especially if one wants to predict the track settlement numerically.

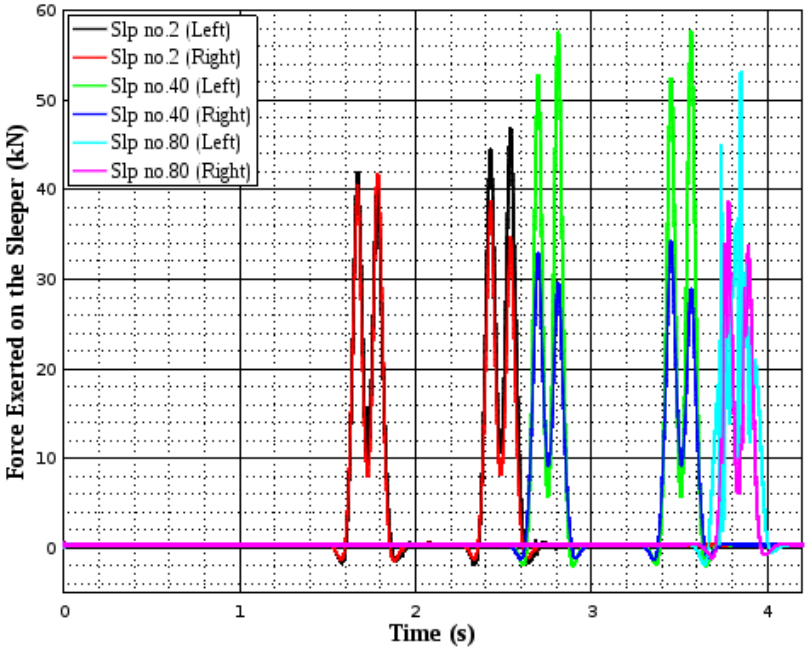

Figure 2-m: Force exerted on the sleeper

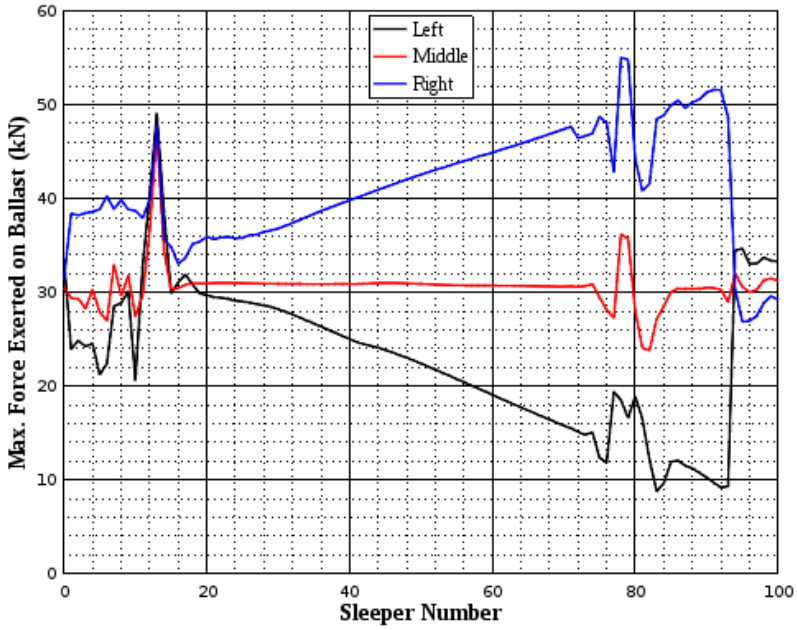

Figure 2-n: Maximum force exerted on the ballast

This page is intentionally left blank.

3. Numerical train-turnout optimization

In the recent years, because of the advancement in computer technology, numerical design optimization has been a popular topic in many fields as well as in engineering field. One of the most prominent advantages of design optimization is that it can perform repetitive studies to find the best solution without much human involvement. This can help to save time to solve problems which might require many iterations in order to find the solution.

Design optimization has been a technique that is very attractive in train-track dynamic field to find the best and optimum design. Some of the optimization examples are optimizing the geometry of the crossing nose [10, 16], switch rail geometry [11, 17], track gauge of the switch panel [18], vertical elasticity of the crossing panel [19], etc. Nevertheless, most of the optimization works carried out are either not considering switch and crossing as a whole, or rather simplified track dynamics without considering the discretization of the rail support condition.

One of the tasks in this study is utilizing the newly developed full train-turnout model to optimize railpad vertical stiffness. Railpad as illustrated in Figure 3-a is an elastic component inserted between rail and sleeper to provide more elasticity to the track and to damp the dynamics of the track induced by the train. Other benefits of using railpads are increase load distribution over a larger surface on the sleepers, avoiding load concentration, reducing noise and vibration.

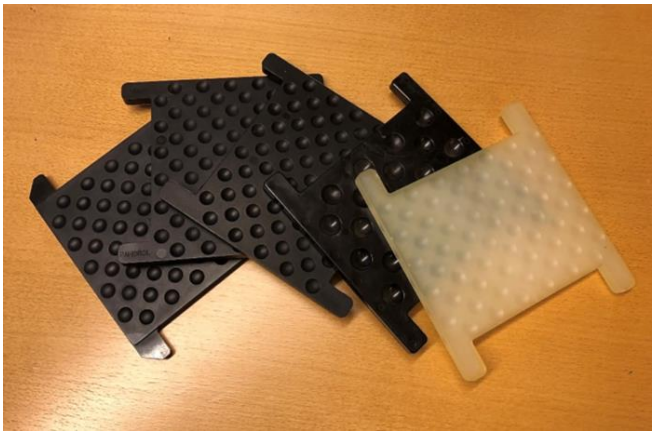

Figure 3-a: Railpads

Traditionally railpad stiffness is kept homogenously along a turnout. However, due to the nature of turnout such as difference in rail bending stiffness and geometry variation, homogenous stiffness will not give optimum performance. Wan et al. [19] utilized numerical modelling tool and an optimization technique to investigate the effect of non-homogenous vertical stiffness along a crossing nose and it is concluded indeed by doing so, a better performance crossing nose can be obtained. However, numerical model used in the work is only a 2D model in a crossing panel of which for a complex turnout component is not always

enough. Inspired by the work, a similar optimization task attempting to find optimized non-homogenous railpad stiffness in the turnout has been carried out. Unlike Wan et al., a full train-turnout model modelled using the track modelling approach discussed in chapter 2 is used. Besides, the optimization technique used in the optimization task is genetic algorithm. The setup of the optimization task is briefly discussed in the following sections.

3.1 Train-turnout model simulation improvement

Usually optimization task involves repetitive simulations in order to find the optimum solution. For example, the optimization task for each case in this study takes around 1500 simulations. The number of simulation normally depends on complexity of the problem Therefore, it is important to ensure that the train-turnout model takes the least amount of time to simulate before it is used for the optimization task. Two major improvements have been implemented on the model simulation before the optimization task.

The first improvement of the model simulation is removal of initial transient effect of the model. As discussed earlier in section 2.3, a 60 m straight track has to be included in the train-turnout model in order to damp the initial transient effect of the train. Although including this 60 m straight track section is important in order to ensure the accuracy of the result, it is actually trivial for all the simulations to simulate this section if the initial condition is the same. To avoid the repetition, only one simulation has been simulated for the first 60 m straight track in the very first simulation of the optimization task. The train and the track dynamics is more or less in the steady state after the train travelling on the straight section for about 31 m. For the subsequent simulations, the train starts at 31 m instead of 0 m with the state of dynamic of 31 m simulated from the first simulation. Figure 3-b illustrates the position of the train in the first simulation compared to the subsequent simulations and their corresponding vertical wheel force. In this way, 31 m less track need to be simulated and this can save a large amount of simulation time.

The second improvement is so-called initiation removal. In GENSYS, before the time simulation, masses and couplings of the model always need to be initiated. This is an essential stage for the software to realize the position of the masses and where they are coupled in the continuum. The time for the initiation is proportional to the amount of masses and coupling in the model. For a full train-turnout model developed for this study, the masses and couplings are a lot more compared to the normal moving mass model. The initiation time for this model is as much as 25 minutes in addition to the time simulation which takes around 15 minutes without the transient effect removal for a laptop computer with Intel core i7-4600U, 4 CPUs, @2.1GHz with 16GB ram. Hence, a separate algorithm has been written to avoid this initiation process. The concept is that, the algorithm saves the initiation of the train-turnout model as a text file in a specific location on the first simulation. Then, the same initiation file is used for the rest of the simulations. For any changes, only the differences are replaced in the initiation file without reinitiating the entire model. With this method, the initiation time can be reduced from 25 minutes to less than 15 seconds.

When these two simulation improvements are deployed, the total simulation time for each simulation is reduced from 40 minutes to only 10 minutes.

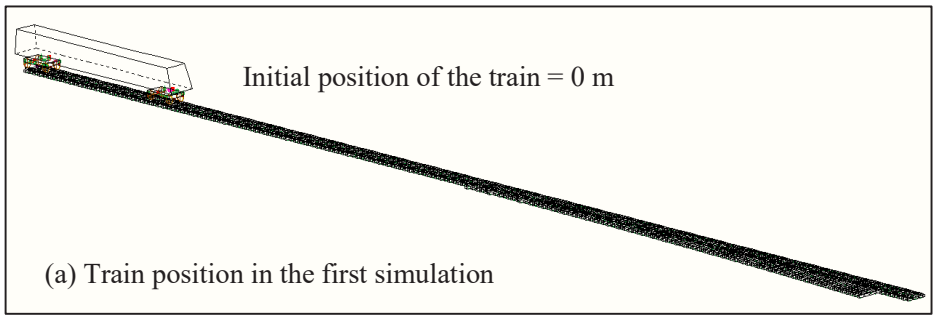

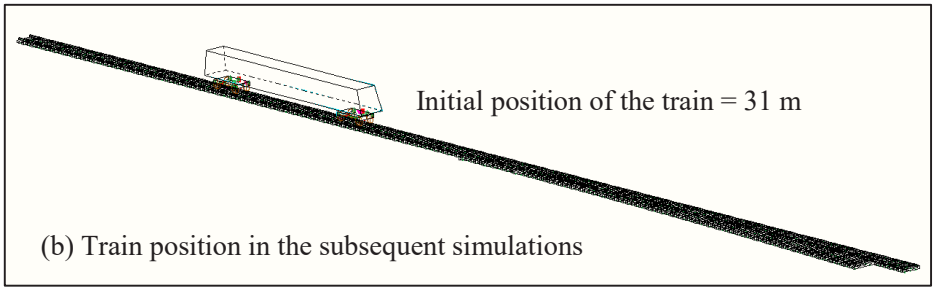

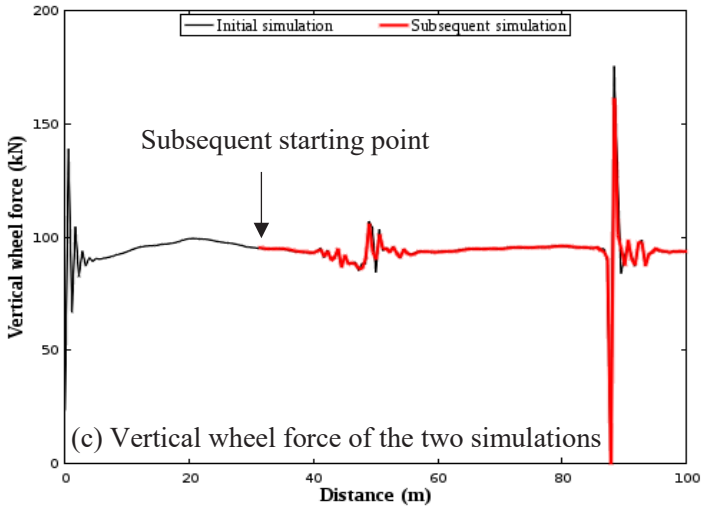

Figure 3-b: Transient effect removal

3.2 Optimization process

The first step for the optimization process is to formulate the problem numerically. One way of formulating is to minimize a function as shown in equation (1). This function in optimization is also called objective function.

$$F(\boldsymbol{x}) \rightarrow min \tag{1}$$

Where $\boldsymbol{x}$ is the design variables.

$$\boldsymbol{x} = [x_1, x_2, x_3 \dots x_n]^T \tag{2}$$

There can be as many design variables as one would like to consider and it can be any parameter in the model. In this study, the design variables are the vertical railpad stiffness in different zones in the turnout as defined in figure 3-c. The definition of the zone is based on the panel definition. However, two different zones are considered instead of one in the crossing panel because the rail in crossing nose in the crossing panel and the rail in opposite side of the crossing nose have large variation in terms of rail bending stiffness.

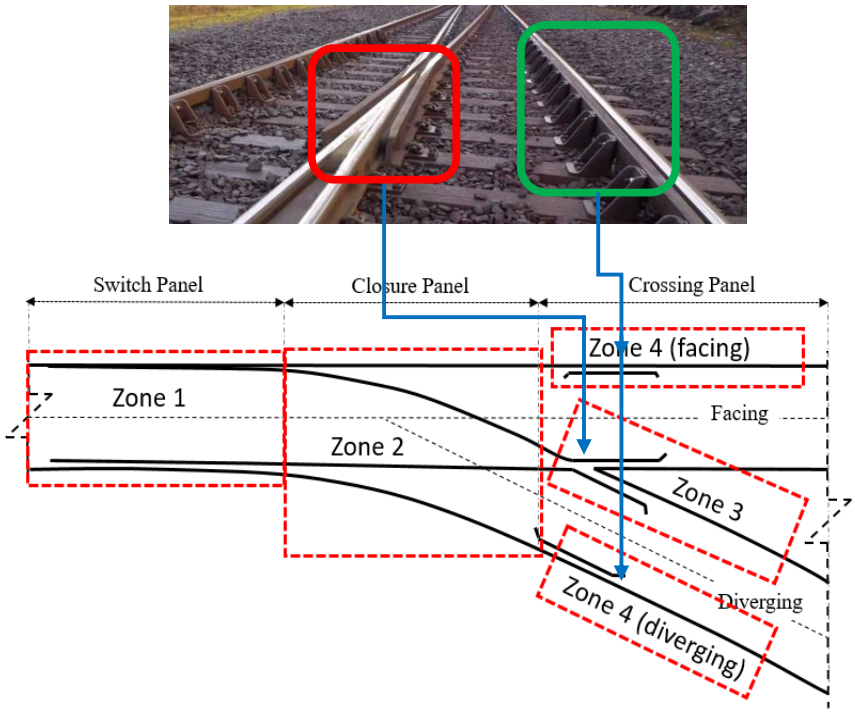

Figure 3-c: Zone definition

Then, each design variable is subjected to side boundary conditions:

$$A_i \leq x_i \leq B_i, \qquad i = 1, \dots, n \tag{3}$$

Where A and B are lower bound and upper bound of the variable respectively.

Definition of assessment criteria is the next task. Similarly, one can consider as many criteria as one would like to assess when formulating the optimization problem. One way of including more than one criteria to be assessed is normalizing the criteria with its reference value and multiplying it with a weighting factor.

$$F(\boldsymbol{x}) = \sum_{i=1}^{m} w^i \frac{f_i}{f_i^r} \tag{4}$$

Where m is the number of criteria to be assessed, w is the weighting factor and the summation of w is equal to one, f_i is the current criteria and f_i^r is the reference value. The benefit of formulating the assessment criteria this way is that the importance of the criteria can be adjusted flexibly. For example, higher weighting factor for the criteria that is more important. In this study, two criteria namely vertical wheel-rail force and maximum force exerted on the sleeper in different zone have been considered. Thus, in total, eight criteria have been considered. A weighting factor of 0.125 is used for all the assessments representing all the criteria are assumed to be equally important.

To ensure the feasibility of the design, a penalty function technique has been used to handle the constraints of the problem.

$$F_p(\boldsymbol{x}) = F(\boldsymbol{x}) + \sum_{j=1}^{k} C_j \left(\frac{\emptyset}{\emptyset_{allow}}\right)_j^2 (\boldsymbol{x}) \tag{5}$$

Where $F_p(\boldsymbol{x})$ is the updated penalized objective function, $F(\boldsymbol{x})$is the unpenalized objective function, C_j is the penalty coefficient, k is the number of constraints, $\emptyset/\emptyset_{allow}$ is the normalized constraint. In this study, the constraint that has been considered is maximum vertical compressive displacement of the railpad. The concept is that, when one or more constraints are violated, a penalty value is to be added to the objective function.

With the above setting, the problem can be solved by the help of an optimization technique. The optimization technique used in this study is genetic algorithm (GA). GA is an optimization technique based on a natural process that mimics biological evolution [20]. One of the advantages of GA is, it is a non-gradient based optimization technique. For non-linear train-track dynamics problem, GA is less likely to converge to a local minimal compared to other gradient-based solvers. GA has been also successfully used in both engineering and non-engineering applications.

One of the challenges in this study is coupling between GA with the train-track modelling tool GENSYS because they do not operate on the same programming platform. The GA used in this study is a pre-written algorithm, optimization tool embedded in MATLAB. GENSYS on the other hand, is an independent program function only in Unix operating system. To overcome this challenge, a separate algorithm is developed to make these two platforms communicate with each other via several text files. The communication process is briefly illustrated figure 3-d. Firstly, GENSYS is fed by a text file with the design variable vectors generated by MATLAB. Then GENSYS simulates the train-track dynamic of the given variables and send MATLAB with a text file that contains information in vector form that needs to be evaluated. This process repeats until the convergence or pre-defined stopping criteria in GA is achieved.

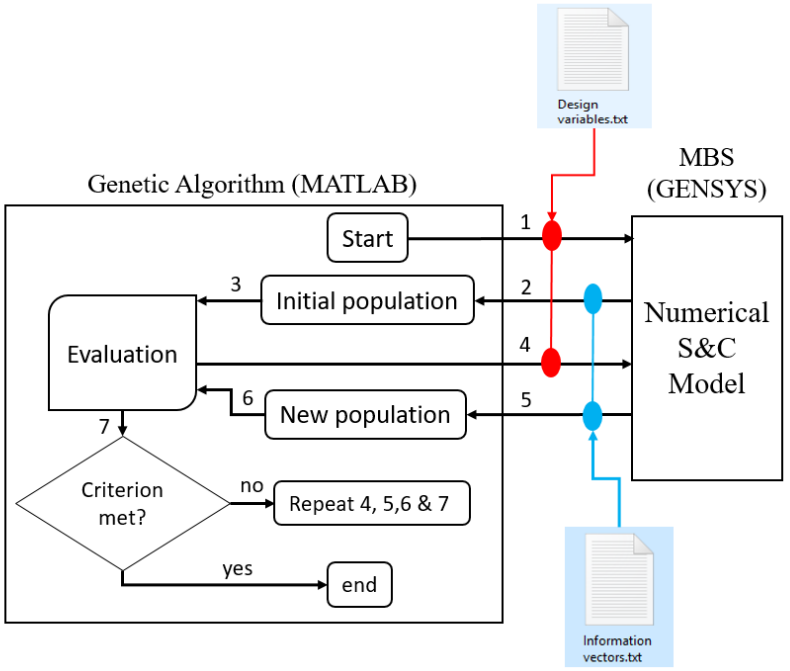

Figure 3-d: MATLB - GENSYS communicating process

Another challenge is the pre-defined stopping criteria in the GA. This is because the function (train-track system) takes rather long time to solve. Over-defining the stopping criteria could result in long simulation time or under-defining the stopping criteria could result in non-optimum result. To overcome that, the stopping criteria are tested with more variables i.e. railpad stiffness and under sleeper pad stiffness (***Paper C***) before the stopping criteria are applied to only railpad vertical stiffness. This is done on the basis that if the stopping criteria are able to find the optimum solution for a problem with eight variables, so theoretically, for the railpad vertical stiffness task of which only four variables are involved, the setting should be sufficient.

3.3 Optimization results

Complete results of the numerical optimization task can be found in the ***Paper D***. However, as a preview purpose, some key results have also been presented here.

The first result is the vertical wheel forces on the leading wheelset before and after optimization when the freight train traveled through the diverging route of the turnout, see figure 3-e. Significant vertical wheel force reduction can be observed when the optimized railpad stiffness is adopted in the turnout. The reduction is more obvious in the switch and crossing panels compared to the closure panel. This is probably because the dynamics of the vertical wheel force is quite significant in these regions and the soft railpads are good in damping the dynamics. Similarly, the dynamic vertical wheel force has been reduced more significantly in the switch and crossing panels on the right wheel compared to the closure panel. This highlights the importance of having non-homogenous railpads stiffness along the turnout.

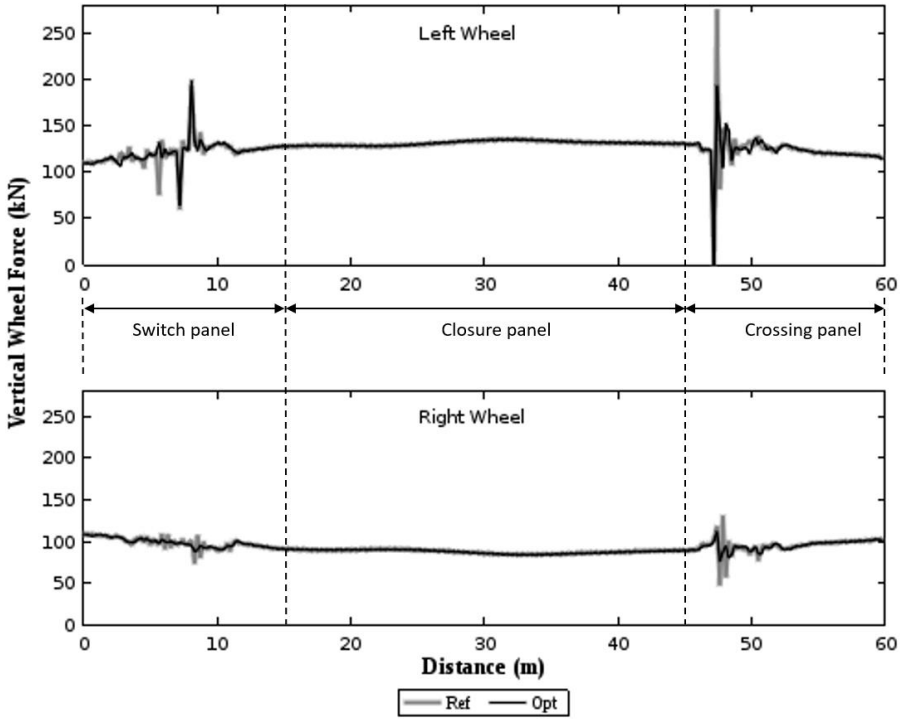

Figure 3-e: Vertical wheel force in diverging direction

The second result is the force exerted on the sleepers. Figure 3-f shows the forces exerted on the sleeper 2 (entrance of the switch panel), sleeper 40 (middle of the closure panel) and sleeper 80 (entrance of the crossing panel) when the train travelled though the turnout in the facing direction.

Significant reduction of the force exerted on the sleeper can be observed in number 2 and 40. Due to low bending stiffness of the rail in the closure panel, the wheel force transferring down to the sleepers in this region is slightly higher compared to sleeper number 2 and 80. The magnitude of the force reduction at sleeper 80 is the lowest despite of having the lowest railpad stiffness out of all the three sleepers. This is probably because the force exerted on the sleeper is already low due to the high bending stiffness of the crossing nose and the soft railpad can only contribute limitedly to the reduction.

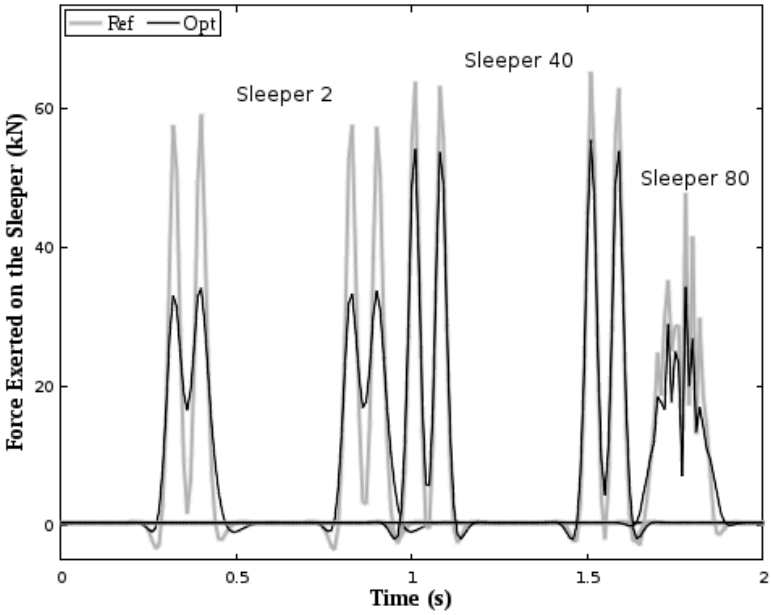

Figure 3-f: Force exerted on the sleeper under the left rail in diverging direction

4. Conclusion

Previously train-track modelling in multi-body simulation (MBS) has been rather simplified. Two of the simplifications are neglecting yaw effect of the wheelsets and use of moving mass track model in the simulation. These simplifications are acceptable if only train dynamics is of interest but not track dynamics. Since track is the focus in this work, two improvements which specifically addressing these simplifications have been achieved.

The first improvement is including wheelset yaw effect into train-track modelling in the MBS environment. The yaw effect is achieved by yawing the 2D wheel profile by transformation in addition to a complex contact information editing procedure done in offline contact calculation module in GENSYS. It is concluded that the yaw of the wheelset has effect towards the flange contact position especially at the entrance of a tight curve and turnout. This effect has direct consequences towards prediction of flange climbing derailment. It is also concluded that for curve and turnout with curvature more than 760 m, the yaw effect of the wheelset is no longer significant and can be neglected in the simulation.

The second improvement is better modelling of track model in the MBS environment. Unlike conventional way of track modeling in MBS which only model railway track as a lumped mass, an approach that is able to model the railway track as a full track model has been developed. The full track model is able to include track properties that cannot be included before such as rail bending stiffness, rail bending stiffness variation and sleeper geometry. A full right hand 60EI-R760-1:15 turnout has been modelled using this modelling approach. It is concluded that the train-turnout dynamics of the full turnout model is in good agreement with the turnout model modelled with the conventional track modelling. It is also concluded that it is important to model turnout in full because factors such as rail bending stiffness difference and sleeper mass variation along the turnout has effect towards the overall dynamics of the train and the track. On the other remarks, with the full track model, time history of the track such as force exerted on the sleepers, sleeper displacement, force exerted on the ballast can be simulated. This also makes other track related analysis such as railway track settlement analysis, sleeper acceleration, and inclusion of ballast characteristic in the future possible.

After that, an attempt has been made to optimize railpad stiffness of the turnout model. The idea is to divide the turnout into different zone and use different railpad stiffness within these zones. The division of the zone is according the rail bending stiffness along the turnout. By utilizing an optimization algorithm namely genetic algorithm, with the aim to reduce the wheel-rail contact force and to reduce force exerted on the sleeper, a guideline of the railpad stiffness of the turnout under this zone customization has been suggested. It is also anticipated that by having such customization and optimization setup, other type of turnout can be optimized too in the future. It is also concluded that it might be safe to use railpads with stiffness 33MN/m homogenously along 60EI-R760-1:15 turnout as long as the allowable axle load of the train is less than 22.5 ton and the train is not travelling faster than 200km/h.

This page is intentionally left blank.

5. Future work

Possible future works after this study are as below:

1. Use a better wheel-rail contact prediction, possibly 3D wheel and rail profiles instead of only 2D. Perhaps integrating the state-of-the-art CONTACT calculation in the model especially modelling a turnout.

2. Improvement on bending stiffness variation capability of the track model as currently the variation can only be varied element-wise (at every support distance).

3. Include structural flexibility of the bodies especially in wheelset. Because some of the wheelset resonance frequencies can be very close to sleeper passing frequency.

4. Further validate the turnout model with a real turnout on-site. Suggestion for the tuning is through receptance test on several points on the turnout.

5. To validate the optimization results obtained from the numerical optimization on-site on a real turnout.

Reference

[1] A. H. Løhren, and A. K. Buan, “Utrekk Vedlikeholdskostnader KV overbygning 2015”, Jernbaneverket, Norway: 2015.

[2] A. H. Løhren, and K. B. Green, “Feil i Sporveksler 2015”, Jernbaneverket, Norway: 2015.

[3] C. Alves , A. Paixão, E. Fortunato, and R. Calçada, "Under sleeper pads in transition zones at railway underpasses: numerical modelling and experimental validation", *Structure and Infrastructure Engineering*, vol. 11, no. 11, pp. 1432-1449, 2015.

[4] A. Johansson, B. Pålsson, M. Ekh, J. Nielsen, M. Ander, J. Brouzoulis, and E. Kassa, "Simulation of wheel–rail contact and damage in switches & crossings", *Wear*, vol. 271, no. 1–2, pp. 472-481, 2011.

[5] M. Wiest, E. Kassa, W. Daves, J. C. O. Nielsen, and H. Ossberger, "Assessment of methods for calculating contact pressure in wheel-rail/switch contact", *Wear*, vol. 265, no. 9–10, pp. 1439-1445, 2008.

[6] H. Wang, V. Markine, and I. Shevtsov, "The analysis of degradation mechanism in track transition zones using 3d finite element model," *Proceedings of the Second International Conference on Railway Technology: Research, Development and Maintenance*, Civil-Comp Press, Stirlingshire, UK, 2014.

[7] A. Paixão, E. Fortunato, and R. Calçada, "A numerical study on the influence of backfill settlements in the train/track interaction at transition zones to railway bridges", *Proceedings of the Institution of Mechanical Engineers, Part F: Journal of Rail and Rapid Transit*, 2015.

[8] E. Kassa, and J. Nielsen, "Dynamic interaction between train and railway turnout: full-scale field test and validation of simulation models", *Vehicle System Dynamics*, vol. 46, no. sup1, pp. 521-534, 2008.

[9] R. Lagos, A. Alonso, J. Vinolas, and X. Pérez, "Rail vehicle passing through a turnout: analysis of different turnout designs and wheel profiles", *Proceedings of the Institution of Mechanical Engineers, Part F: Journal of Rail and Rapid Transit*, 2012.

[10] C. Wan, V. Markine, and R. Dollevoet, "Robust optimisation of railway crossing geometry", *Vehicle System Dynamics*, vol. 54, no. 5, pp. 617-637, 2016.

[11] B. Pålsson, "Design optimisation of switch rails in railway turnouts", *Vehicle System Dynamics*, vol. 51, no. 10, pp. 1619-1639, 2013.

[12] A. Lau, and E. Kassa, "Simulation of vehicle-track interaction in small radius curves and switches and crossings", *Proceedings of The Third International Conference on Railway Technology: Research, Development and Maintenance*, 2016.

[13] GENSYS user's manual, release 1701. Available from: www.gensys.se

[14] T. Dahlberg, "6 Track Issues", *Handbook of railway vehicle dynamics*, 2006.

[15] E. Kassa, C. Andersson, and J. C. Nielsen, "Simulation of dynamic interaction between train and railway turnout", *Vehicle System Dynamics*, vol. 44, no. 3, pp. 247-258, 2006.

[16] B. Pålsson, "Optimisation of railway crossing geometry considering a representative set of wheel profiles", *Vehicle System Dynamics*, vol. 53, no. 2, pp. 274-301, 2015.

[17] P. Wang, X. Ma, J. Wang, J. Xu, and R. Chen, "Optimization of Rail Profiles to Improve Vehicle Running Stability in Switch Panel of High-Speed Railway Turnouts", *Mathematical Problems in Engineering*, vol. 2017, pp. 13, 2017.

[18] B. Pålsson, and J. C. O. Nielsen, "Track gauge optimisation of railway switches using a genetic algorithm", *Vehicle System Dynamics*, vol. 50, no. sup1, pp. 365-387, 2012.

[19] C. Wan, V. Markine, and I. Shevtsov, "Optimisation of the elastic track properties of turnout crossings", *Proceedings of the Institution of Mechanical Engineers, Part F: Journal of Rail and Rapid Transit*, vol. 230, no. 2, pp. 360-373, 2016.

[20] L. Davis, "Genetic Algorithms and Simulated Annealing", 1987.

Paper A

"Simulation of vehicle-track interaction in small radius curves and switches and crossings"

A. Lau and E. Kassa

Proceedings of the Third International Conference on Railway Technology: Research, Development and Maintenance, Cagliari, 2016.

Is not included due to copyright

Paper B

"Simulation of train-turnout coupled dynamics using a multibody simulation software"

A. Lau and I. Hoff

Submitted for publication, in Modelling and Simulation in Engineering by Hindawi, 2017.

Simulation of Train-turnout Coupled Dynamics Using a Multibody Simulation Software

Albert Lau and Inge Hoff

Department of Civil and Environmental Engineering, Norwegian University of Science and Technology, Trondheim, Norway.

Correspondence should be addressed to Albert Lau; albert.lau@ntnu.no

Abstract

With the advancements of computing power, multibody simulation (MBS) tool is not only used to study train dynamics, but more realistic phenomena such as train-track coupled dynamics. However, train-turnout coupled dynamics within MBS is still hard to be found. In this paper, a train-turnout coupled model methodology using a MBS tool GENSYS is presented. Dynamic track properties of a railway track is identified through numerical receptance test on a simple straight track model. After that, the identified dynamic track properties are adopted in a switch and crossing (turnout) to simulate train-turnout coupled dynamic interaction including parameters such as rail bending stiffness and sleeper mass variation along the turnout. The train-turnout coupled dynamic interaction is compared to the dynamic interaction simulated from a widely accepted moving mass train-turnout model. It is observed that the vertical and lateral normal forces for the new train-turnout coupled model and the conventional moving mass train-turnout model are in good agreement. In addition, the new train-turnout coupled model can provide additional track dynamics results. It is concluded that the train-turnout coupled model can provide a more realistic train-turnout dynamic interaction compared to the moving mass train-turnout model.

Keywords: train-turnout coupled interaction, multi-body dynamics, switch and crossing, turnout

1. Introduction

A good understanding of the train and track dynamic interaction is important to optimize design and maintenance of the track components. Switches and crossings are of special interest because of the increased loading that causes extra wear and high maintenance costs. Train and track dynamic simulations are used to study how train or track reacts when they are subjected to different conditions such as different axle loads, traveling speed, and track geometry especially at the design and development stages. Through train and track dynamic analysis, it is possible to evaluate how modifications in train and/or track affect several factors such as riding comfort, vehicle or track accelerations, derailment risk, rolling contact fatigue, rail

stresses, rail deflection, etc. On top of that, numerical simulations reduce reliance on experimental campaigns that in most cases can be very expensive and time consuming.

Two types of numerical methods are most commonly used in the quest of simulating train or/and track dynamics i.e. multibody simulation (MBS) method and finite element method (FEM). Since the train-track complicated when it comes to dynamics, geometry and material behavior, it is necessary to make simplifications to be able to build the model and run the simulations in a reasonable time. The MBS-method is known to be efficient to study the train dynamics but the trade-off is the track model has to be simplified. In the FEM, a very detailed train-track model can be modelled including bodies' structural flexibility; however, the computational effort is much higher compared to MBS. Therefore, FEM in railway field often used only for very detailed component modelling [1], detailed wheel-rail contact modelling [2, 3], etc. Sometimes FEM is also used for train-track simulation as a whole, but simplifications are often made to reduce the computational effort [4, 5].

MBS is preferable to study train-track dynamic interaction as a whole, especially for complex railway track component such as switch and crossing. MBS tool dedicated for train-track analysis has a wheel-rail contact module that is able to model complex wheel-rail kinematic behaviour and the corresponding creep forces. Some authors, for example Kassa et al.[6], Lagos et al.[7], Wan et al.[8], Pålsson[9], and Lau et al.[10] used MBS to simulate train-turnout dynamic interaction to evaluate the maximum contact forces along a railway turnout, to study the influence of the turnout geometry, to optimise crossing nose profile, to optimise switch geometry and to study the effect of yaw in a switch and crossing respectively. As reported by Esveld [11], the track substructure has a direct influence on the dynamic wheel load, dynamic track stiffness, and track roughness. However, to model railway track in MBS has always been a challenge [12]. Moreover, the train-turnout model used by the abovementioned authors are moving mass train-turnout model of which the track is represented by a lumped mass or mass layers coupled using spring-damper elements and the track follows the train's wheels throughout the simulation. Such track model is able to capture dynamics up to 200Hz. Some frequencies such as sleeper passing frequency and frequencies induced the rail bending stiffness are not able to be modelled. Moreover, constant sleeper mass is used even though in reality sleeper mass is not the same along switches and crossings.

In the present paper, a train-turnout coupled model using a MBS software GENSYS is presented. Dynamic track properties is first determined using a simple straight track model through receptance test by referring to existing receptance functions recorded in the literature. After that, the determined track properties are applied to a turnout model. The train-turnout coupled model is simulated and the corresponding dynamic interaction is compared to the dynamic interaction from a moving mass

train-turnout model. Some track dynamics of the train-turnout coupled model are also reported. Benefits and drawbacks of the model are discussed in the paper.

2. Train model

Train model presented in this paper is a Norwegian passenger train represented by seven bodies i.e. a carbody, two bogies and four wheelsets. Each of the bodies has six degrees of freedom (DOF) i.e. three translations and three rotations apart from the wheelsets which have only five DOFs with longitudinal translation being constrained. The bodies are coupled to each other with spring-dampers elements. Unlike conventional moving mass model, the train model in this paper is modelled in a moving coordinate system relative to the track fixed coordinate system. Figure 1 illustrated a schematic drawing of the train and the track model.

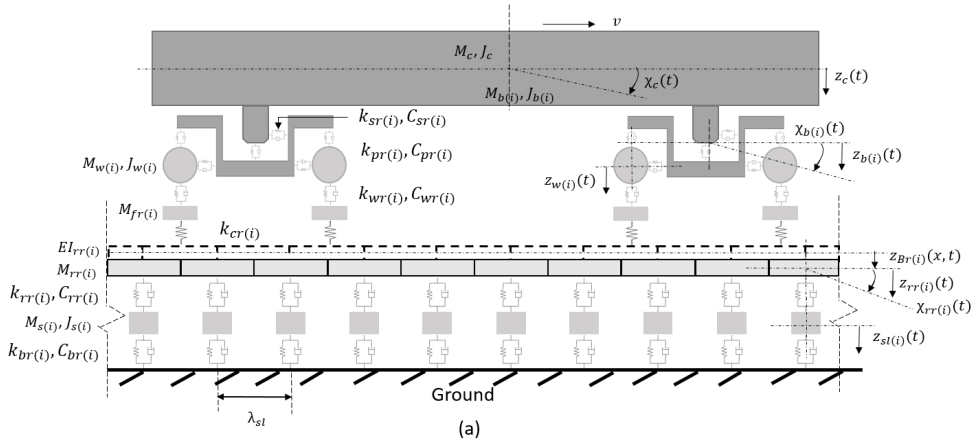

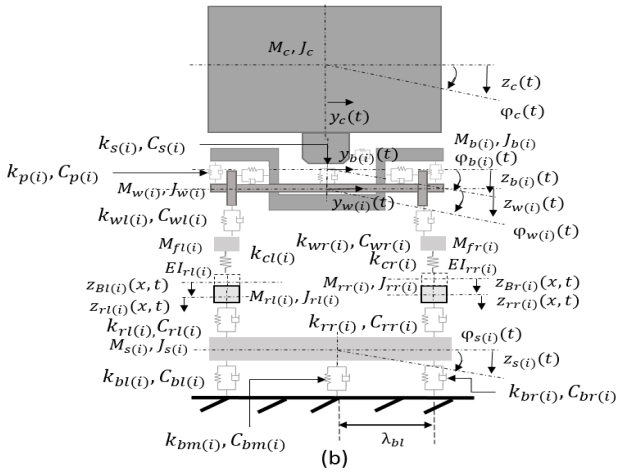

Notations	
v – wheelset velocity	EI_r –rail bending stiffness
Second subscript l - left position	k_r –railpad stiffness
Second subscript r - right position	c_r – railpad damping
Second subscript m - middle position	k_b –ballast stiffness
Subscript (i) – item number	c_b –ballast damping
M_c – carbody mass	z_c – carbody vertical displacement
J_c – carbody mass inertia	z_b – bogie vertical displacement
M_b – bogie mass	z_w – wheelset vertical displacement
J_b – bogie mass inertia	z_s – sleeper mass vertical displacement
M_w – wheelset mass	y_c – carbody lateral displacement
J_w – wheelset mass inertia	y_b – bogie lateral displacement
M_f – fictitious rail mass	y_w – wheelset lateral displacement
M_r – rail mass	z_B – rail (beam) vertical displacement
J_r – rail mass inertia	z_r – rail mass vertical displacement
M_s – sleeper mass	φ_c – carbody roll rotation
J_s – sleeper mass inertia	φ_b – bogie roll rotation
k_s – secondary suspension stiffness	φ_w – wheelset roll rotation
c_s – secondary suspension damping	φ_s – sleeper mass roll rotation
k_p – primary suspension stiffness	χ_c –carbody mass pitch rotation
c_p – primary suspension damping	χ_b –bogie mass pitch rotation
k_w – wheel-fictitious rail contact stiffness	χ_r –rail mass pitch rotation
c_w – wheel-fictitious rail contact damping	λ_{sl} – sleeper distance
k_c – fictitious rail-rail contact stiffness	λ_{bl} – ballast support distance

Figure 1: Schematic drawing of the train-track model [Not to scale]; (a) Side view, (b) Rear view.

3. Turnout model

3.1 Track modelling

There have been some attempts to model railway track using MBS for example in [13, 14, 15]. One of the most popular way of modelling railway track is modelling rail of the track as a beam element using the Euler-Bernoulli beam theory. State of the general dynamic beam equation, rail in this case can be expressed by Euler-Lagrange equation.

$$L = \frac{1}{2}\rho A\left(\frac{\partial w}{\partial t}\right)^2 - \frac{1}{2}EI\left(\frac{\partial^2 w}{\partial x^2}\right)^2 + q(x,t)w(x,t) \tag{1}$$

Where ρ is the mass density, A is the cross-section area, E is the elastic modulus and I is the second moment of area of the beam's cross-section. Since Euler-Bernoulli beam can only be supplied with the load and provide deflection in vertical direction, $q(x,t)$ is the external load and $w(x,t)$ is the deflection of the beam in vertical direction at time t along the longitudinal position x. The external load $q(x,t)$ is the excitation and the corresponding reaction generated by the train (wheel) on the top of the beam and is expressed as:

$$q(x,t) = -\sum_{i=1}^{N_s} R_i\delta(x - x_i) + \sum_{j=1}^{N_w} F_j\delta(x - x_j) \cdot \left[H\left(t - t_j\right) - H\left(t - t_j - \Delta t_j\right)\right] \tag{2}$$

Where N_s is the number of supports, which in this case is modelled as a body rigidly connected under the beam with vertical translation and rotation in pitch direction unconstrained, R_i is the i^{th} support reaction force, $\delta(\cdot)$ is the Dirac delta function, x is the current position, x_i is the support position, N_w is the number of wheels travelling over the beam, F_j is the wheel-rail contact force under the j^{th} wheel, $H(\sim)$ is the unit step function, t is the current time step, t_j is the inbound time of the j^{th} wheel at the beam, Δt_j is the time travelled of the j^{th} wheel through the beam. Since

$$\frac{\partial L}{\partial w} = \frac{\partial}{\partial t}\left(\frac{\partial L}{\partial \dot{w}}\right) + \frac{\partial^2}{\partial x^2}\left(\frac{\partial L}{\partial w_{xx}}\right) \tag{3}$$

Euler-Lagrange equation can be expressed as:

$$q(x,t) = \rho A \frac{\partial^2 w}{\partial t^2} + C \frac{\partial w}{\partial t} + EI \frac{\partial^4 w}{\partial x^4} \quad (4)$$

Where C is the viscous damping coefficient. Through modal superposition, the vertical deflection $w(x,t)$ can be expressed by:

$$w(x,t) = \sum_{h=1}^{\infty} A_h(t).S_z(h,x) \quad (5)$$

Where $A_h(t)$ is the h^{th} mode time coefficient of vertical deflection and $S_z(h,x)$ is the h^{th} mode shape function of vertical deflection. Substituting Eq. (5) into Eq. (4) yields:

$$\ddot{W}_h + 2\xi_h\omega_h \cdot \dot{W}_h + \omega_h^2 W_h = \frac{q}{m_h}, \quad (h = 1, 2, \dots, \infty) \quad (6)$$

Where $\omega_h = \left(\frac{h\pi}{L}\right)^2 . \sqrt{\frac{EI}{\rho A}}$ is the model frequency, $\xi_h = \frac{C}{2\rho A\omega_h}$ is the damping ratio and $m_h = \rho A$ is the model mass of the h^{th}mode for a single span beam.

Note that when defining the beam in GENSYS, Euler-Bernoulli beam function is a massless beam and the beam mass is only considered by the rail masses connected rigidly under the beam. This is because these masses are needed to act as bodies that allow more masses such as sleeper masses, ballast masses, etc. to be connected underneath them to represent a more realistic track, see figure 1. Therefore, the Euler-Lagrange equation as stated in equation (1) is only completed when the rail masses rigidly connected under the beam are defined. The rail masses are constrained in every direction apart from vertical translation and pitch rotation. One should be careful when selecting the moment of inertia of the rail masses in pitch direction as it has direct consequences to the bending and deflection of the beam. For instance, if the moment of inertia of the rail masses are too high, the beam will be restricted from bending or the bending and the deflection of the beam will be unrealistically high if the moment of inertia is too low.

For multi-span continuous beam, beam elements are represented by finite beam elements via matrix coupling. For more details of the finite beam elements, refer to N. Ottosen [16]. If needed, for example in switch and crossing, the bending stiffness of the beam can be varied sectionally along the track. The corresponding model frequencies, damping ratio, and models masses can be expressed by complex trigonometric functions. Such approach has previously been successfully implemented by Y. Sun et al. [17] to simulate vertical dynamic of train-rail bridge interaction.

3.2 Track properties validation

One of the most crucial information for the track modelling is the dynamic track properties. Although there is existing information of track properties such as the one recorded in [18], it applies only for moving mass track model. Therefore, a numerical track receptance test is performed on a straight track model (without vehicle) to identify the dynamic properties of the track.

The straight track model for the identification consists of 100 rail masses connects rigidly under two beams (50 on each side). Each pair of rail masses (left and right) are connected to a sleeper mass (a total of 50 sleeper masses) with spring-damper elements representing railpads. Under each sleeper, three spring-damper elements, left middle and right are used to represent the ballast flexibility connecting the sleeper to the rigid ground. The arrangement of the sleeper to rigid ground coupling is such that the left and the right spring-damper elements are always 350mm from the edge of the sleeper and another one is always in the middle of the sleeper. The sleeper masses are constrained in every directions apart from the vertical translation and roll rotation.

Two receptance tests, one on the rail above a sleeper and another in between two sleepers are performed. The corresponding receptance functions are adjusted to match the receptance functions as described in the literature [19] by means of tuning the track parameters such as railpad and ballast stiffness and damping properties.

Since there is no rail mass in the middle of the supports, an approximated method has to be used to obtain the receptance function when the excitation is applied in the middle of two sleepers. The displacement of the rail in the middle of two sleepers, δ_{mid} can be approximated using the pitch angle and displacement of the adjacent rail masses:

$$\delta_{mid}(t) = \delta_i(t) \cdot \lambda_1 + \chi_i(t) \cdot x \cdot \lambda_2 + \delta_{i+1}(t) \cdot \lambda_3 + \chi_{i+1}(t) \cdot x \cdot \lambda_4 \qquad (7)$$

Where δ_i and δ_{i+1}, and χ_i and χ_{i+1} are the vertical displacement and the pitch angle of the masses rigidly connect under the beam adjacent to the point of observation respectively, x is the support distance, and λ is the basis function which can be expressed as:

$$\begin{aligned} \lambda_1 &= 1 - 3 \cdot x_r^2 + 2 \cdot x_r^3 \\ \lambda_2 &= x_r - 2 \cdot x_r^2 + x_r^3 \\ \lambda_3 &= 3 \cdot x_r^2 - 2 \cdot x_r^3 \\ \lambda_4 &= -x_r^2 + x_r^3 \end{aligned} \qquad (8)$$

Where,

$$x_r = \frac{x_0}{x} \qquad [x_0 \ngeq x] \tag{9}$$

x_r is the relative longitudinal position along the beam and x_0 is the distance to the position from the mass on the left of which in the case of observation in the middle of two masses, $x_r = 0.5$, $\lambda_1, \lambda_2, \lambda_3and\lambda_4$ has a value of 0.5, 0.125, 0.5 and -0.125 respectively.

Figure 2 shows the receptance functions of the track with the properties as listed in table 1. It can be seen that the three principal resonance frequencies as mentioned in [19] are captured. The first resonance, which is regarded as track resonance (rails and sleepers vibrate on the ballast) which usually occurs in the frequency range of 50 to 300Hz, is captured at the frequency around 129Hz. The second resonance frequency, which is regarded as the rails bouncing on the railpads and usually occurs in the frequency range of 200 to 600Hz, is captured at the frequency around 485Hz. In this model, pin-pin resonances can also be captured and is at the frequency around 900Hz.

Due to the approximation method (equation 7 – 9), the magnitude of the receptance function on the rail between two sleepers is slightly lower compared to the receptance function on the rail above the sleeper. This is because the displacement and rotation of the rail masses adjacent to the point of observation do not always have the same magnitude and the compromise of the magnitudes leads to slight reduction of the overall magnitude. In addition, the magnitude of the receptance at the pin-pin frequency when the receptance function is observed on the rail between the two sleepers is not as drastic as stated in the literature. This is because the approximation is based on the deflection and rotation of the two adjacent rail masses at the point of observation and the projection is restricted by the rotation magnitude of the rail masses.

A modal analysis of the track as shown in figure 3 is performed to illustrate the corresponding mode shapes of the resonance frequencies. The resonance frequencies from the modal analysis coincide well with the principal resonance frequencies computed from the track receptance tests despite of the linearization of the track model in the modal analysis. Therefore, it is concluded that the track properties are valid to be applied to a more sophisticated turnout model.

Table 1: Track properties

Element	Unit	Value
Euler-Bernoulli beam	Bending stiffness (Nm^2)	6.11×10^6
Rail mass	Mass (kg/m)	60
	Inertia I_x (kgm^2)	1.17
	Inertia I_y (kgm^2)	1.25
	Inertia I_z (kgm^2)	1.15
Railpad	Stiffness (N/m)	300×10^6
	Damping (Ns/m)	50×10^3
Support distance	- (m)	0.6
Sleeper mass	Mass (kg)	380
	Inertia I_x (kgm^2)	4.67
	Inertia I_y (kgm^2)	155.09
	Inertia I_z (kgm^2)	156.12
Ballast	Total stiffness (N/m)	280×10^6
	Total damping (Ns/m)	120×10^3

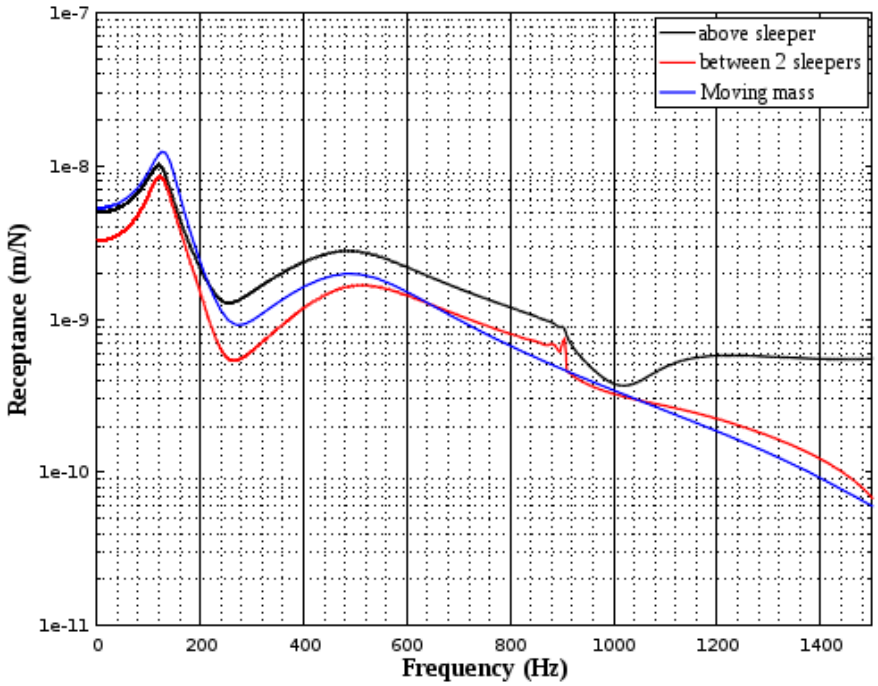

Figure 2: Receptance functions

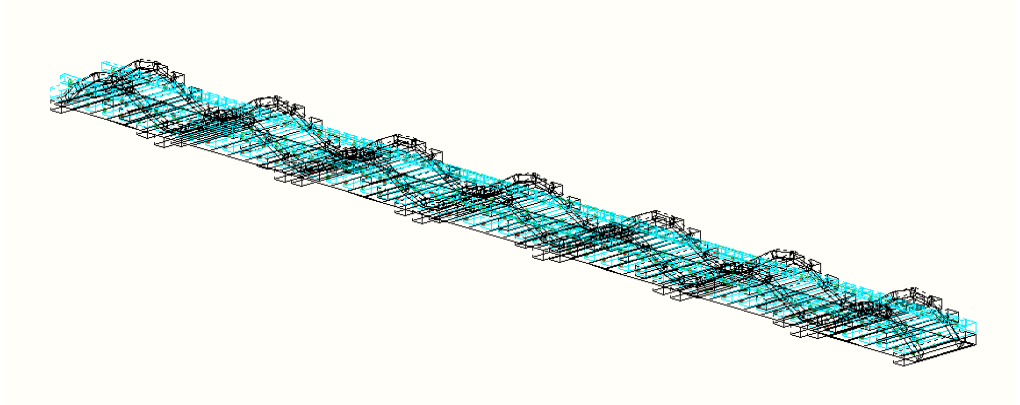

(a)

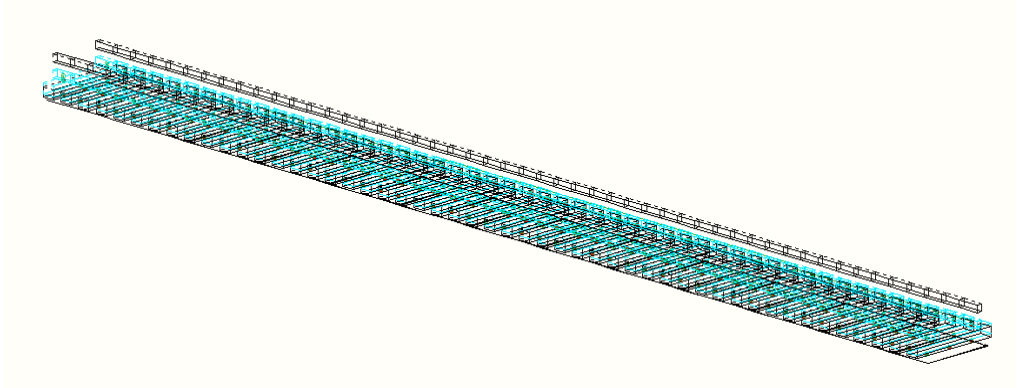

(b)

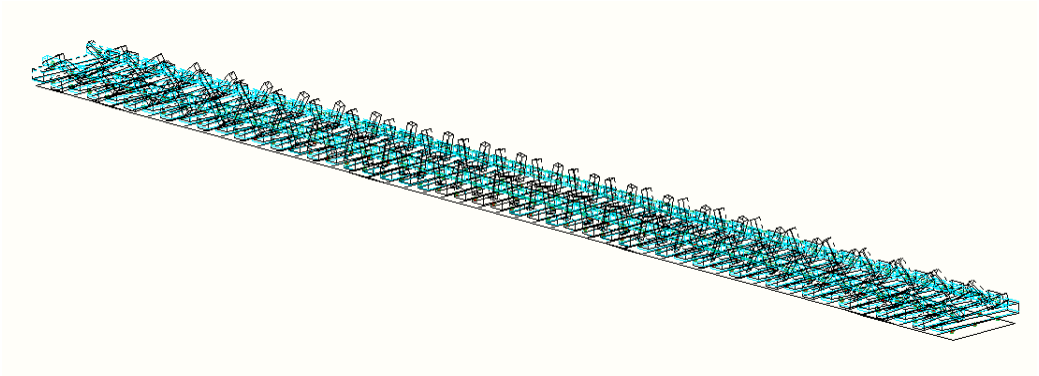

(c)

Figure 3: Mode shapes (a) 129.10Hz (b) 505.08Hz (c) 830.48Hz

In addition, a receptance test is performed on a mass moving track model as shown in figure 4 to achieve a comparable track model with the full track model. The moving mass track model consists of two rail masses coupled to a sleeper mass with spring-damper element and the sleeper mass is connected to rigid ground with two spring-damper elements. Besides, the sleeper mass is also attached to a rigid wall in the lateral direction using a spring-damper element with the value of 30MN/m and 270kNs/m respectively. Apart from the vertical translation, the rail masses and sleeper masses are constrained in every direction.

It can be seen that the track receptance function of the moving mass track model when similar values in table 1 are adopted appears nearly the same as the receptance functions from the full track model. However, the pin-pin resonance in the mass moving track model is missing because of the absence of the beam element. Moreover, one should also note that when the mass moving model is connected to a

train model, the second resonance frequency will not appear because the inertia of the rail masses will not be considered.

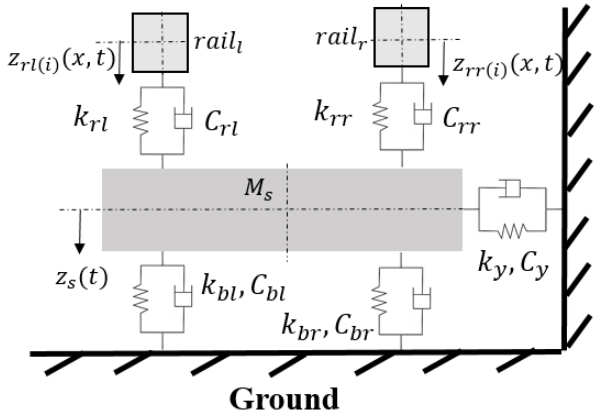

Figure 4: Moving mass track model

3.3 Turnout model

The turnout model is a right turn 60E1-760-1:15 (Nominal rail profile 60E1, curve radius 760m, and turnout angle 1:15) turnout without rail inclination. The variation of the rail profile in the turnout is accounted for by 30 rail cross-sections along the turnout. The total length of the turnout model is 120m. The first 60 m of the track is a straight track modelled to damp the initial transient effect and the rest is the turnout model. This means that, the turnout model consists of 400 rail masses, 200 sleeper masses and 1000 spring-damper elements for the coupling of the rails to the sleepers and to the rigid ground.

Unlike normal track, the rail bending stiffness is varied according to the rail profile in contact with the wheels along the turnout. However, due to the constraints of the Euler-Bernoulli beam equation, the bending stiffness can only be varied sectionally. The bending stiffness of the beam sections are approximated by the mean of the bending stiffness at the closest adjacent measured rail profiles according to the construction drawing. In addition, the sleeper properties such as mass, dimension and moment of inertias are also varied along the turnout according to the construction drawing.

Since the rails are positioned differently on the sleepers along the switch and crossing for facing and diverging route, the rails have to be positioned accordingly in the model for different moving direction (only diverging route is considered in

this work). The rest of the track properties follow the validated track properties as listed in table 1. Figure 5 is a schematic plan view of the turnout model without the 60m straight section.

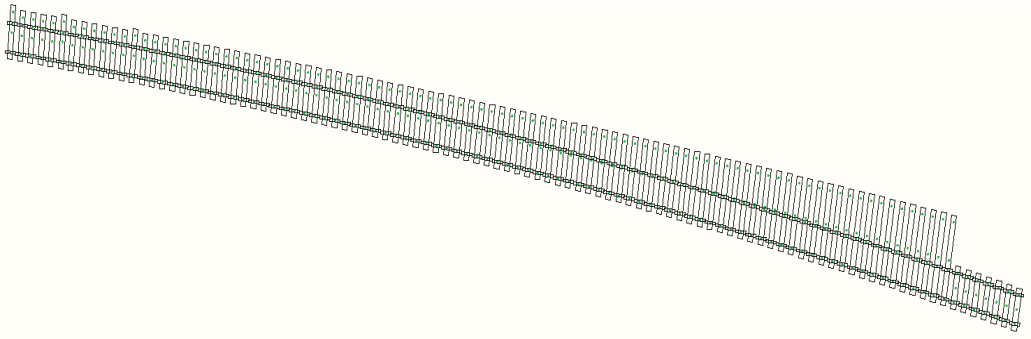

Figure 5: Schematic plan view of the turnout geometry

4. Train – turnout coupling

For the coupling of the train and turnout model, a stiff spring-damper system 141MN/m and 30kNs/m respectively is adopted for each wheel of the train connect to a neglected inertia fictitious mass. The fictitious masses are needed in order to extract wheel-rail profile contact information and any track irregularity during the time simulation, i.e. offline lookuptable is used in the model. The fictitious mass is connected to the Euler-Bernoulli beams by a very stiff 'rail-rail' contact stiffness k_c, which has a value of 5000MN/m assuming the wheel and the rail do not lost contact during the simulation.

For the normal wheel-rail contact problem, Hertz contact theory is adopted. The creepages and creep forces are solved by using the FASTSIM algorithm by Kalker based on the simplified theory of rolling contact. Unlike moving mass track model, the inertia of the rail masses do not need to be neglected because the wheel of the train in the full track model roll over the track without carrying the track under the wheel.

5. Numerical Results

Two simulations have been carried out, train-turnout coupled model and moving mass turnout model. Similar train model and values up to wheel-rail contact are used for the both simulations. The train travelled through the turnout at the speed of

80km/h. The switch panel of the turnout starts at 0 m and the crossing panel starts at around 47 m. The sampling frequency for both simulations is 1000Hz.

Figure 6 shows the vertical normal force of the wheels on the leading wheelset. It can be seen that the vertical normal force are very similar in general for the both models. However, variation can be observed in switch and crossing panels where the dynamic impact is higher. This is probably because the track reacted to the dynamic impact differently and eventually affect the magnitude of the vertical normal force. Similar phenomena can be observed in the lateral normal force as illustrated in figure 7.This can also be explained by the similarity of the vertical and lateral normal forces along the turnout when the dynamic interaction is not as significant. Figure 8 shows the zoomed in vertical normal force. Sleeper passing effect can also be simulated in the train-turnout coupled model but not the moving mass turnout model.

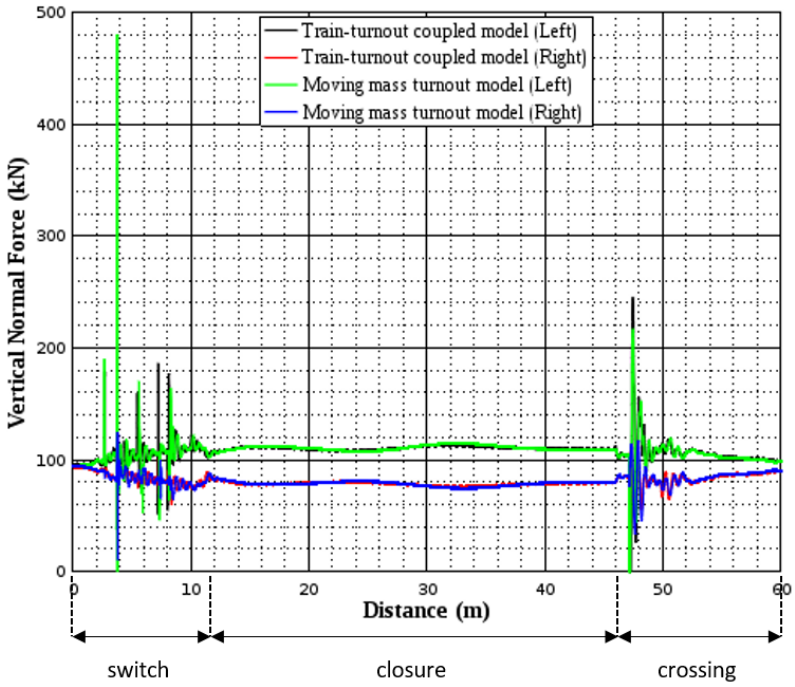

Figure 6: Vertical normal force of the wheels on the leading wheelset

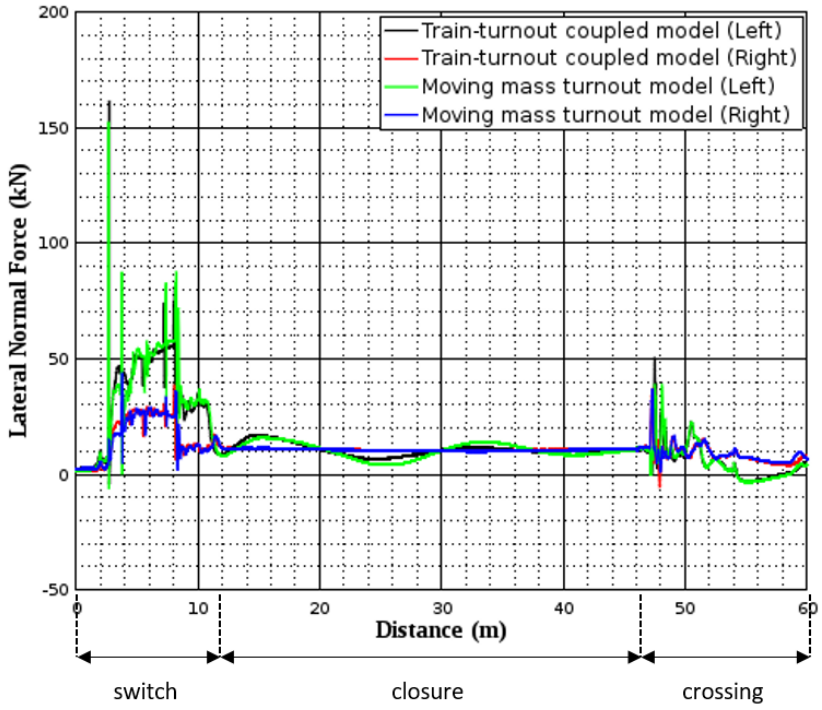

Figure 7: Lateral normal force of the wheels on the leading wheelset

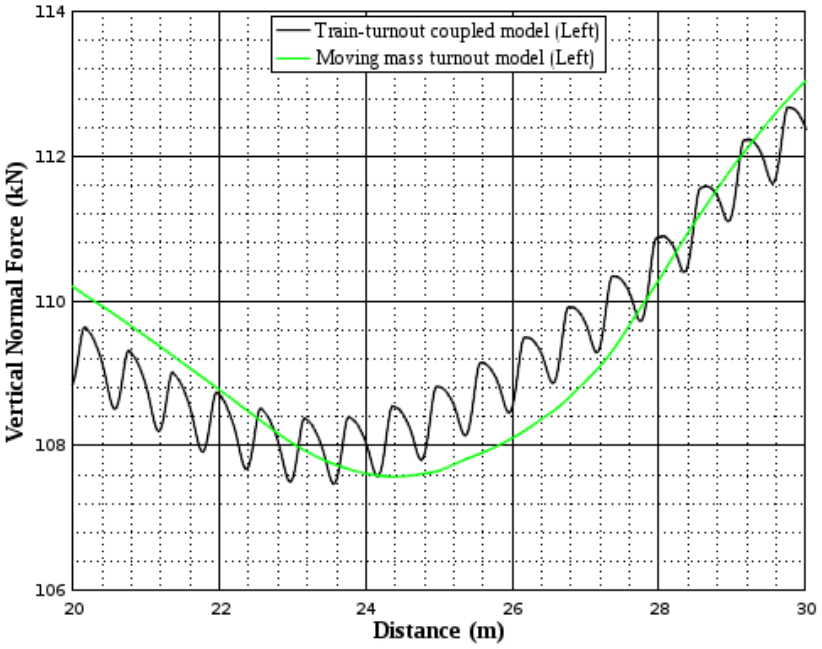

Figure 8: Sleeper passing frequency

Simulating the train-turnout coupled dynamic using this approach, additional information in connection to the track such as the time history of the sleeper, force exerted on the sleeper, sleeper acceleration, and force exerted on the ballast can also be observed. Figure 9 illustrates the forces from the left and the right rail exerted on the sleeper number 2, 40, and 80 near the switch panel, closure panel and crossing panel respectively. All the four wheels passages can be observed in the sleeper number 2 and number 40. However, only first two wheels passages can be observed at the sleeper number 80 due to the length of the track and the trailing bogie did not travel through it before the end of the simulation. It can be seen that the distribution of the forces is even for the first two wheels passage on the sleeper number 2 but the force gradually distributed more to the left wheel when the rear wheels passed the sleeper because of curvature experienced by the train. The curvature effect becomes more obvious at the sleeper number 40. In addition to the curvature effect, the dynamic impact due to the crossing profile in the sleeper number 80 can be observed.

Figure 10 shows the maximum force exerted on the sleepers throughout the turnout. It can be seen that the maximum force exerted on the left rail is higher than the right rail because of the curvature of the track. Besides, highest force exerted on the sleeper is in the switch panel (sleeper number 1 to 20) and the lowest force exerted on the sleeper is in the crossing panel (sleeper number 70 to 90). This is because the bending stiffness of the rail is higher in crossing panel compared to the switch panel. The high bending stiffness of the rail in crossing panel prevent the force from transferring down to the sleepers even though the dynamic impact is high in this region. Although the dynamic impact on the rail in the switch panel is not as significant as in the crossing panel, the maximum force exerted on the sleepers is higher compared to the force exerted on the sleeper in the crossing panel due to the relatively lower bending stiffness of the rail.

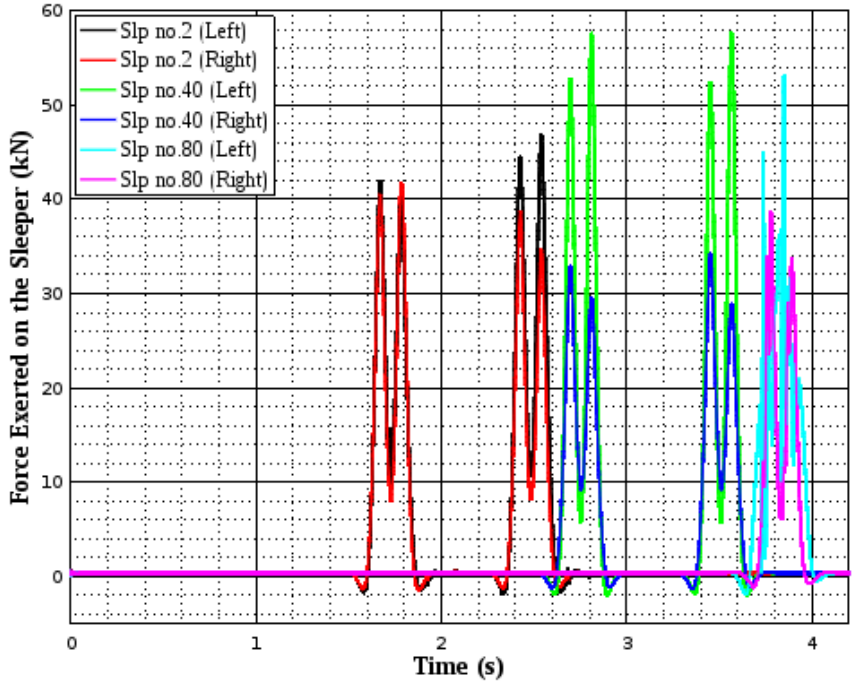

Figure 9: Force exerted on the sleeper

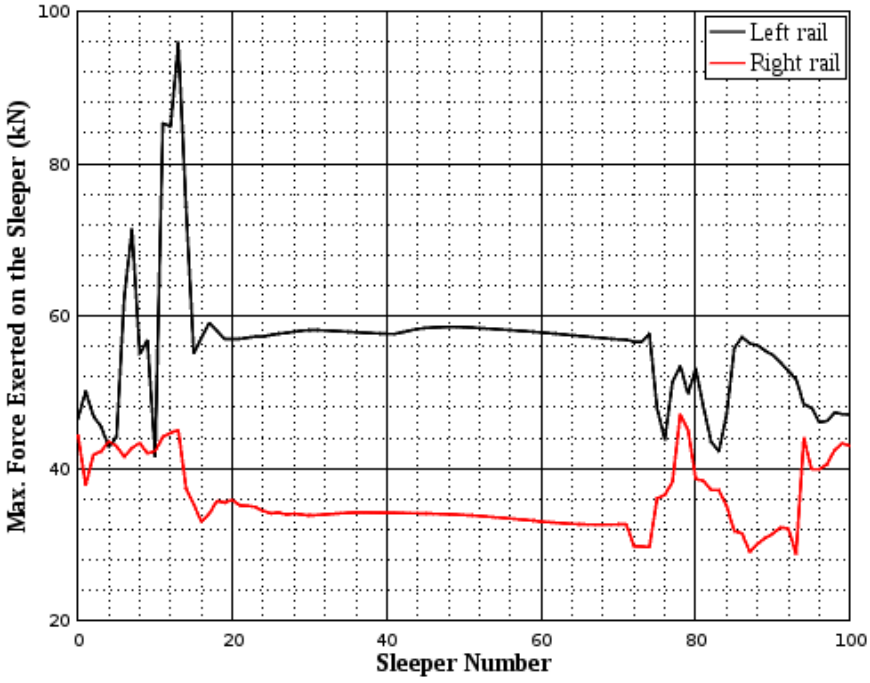

Figure 10: Maximum force exerted on the sleeper

Figure 11 illustrates the forces transfer from the sleepers down to the ballast through the left, middle and the right spring-damper elements under sleeper 2, 40 and 80. It can be seen that the force under the sleepers on the right is higher than the middle and the left in general. This is because formation of the turnout such that the rails are placed gradually rightward along the diverging route. This effect is more obvious at the sleeper number 80, which is near the crossing panel. The force exerted on the ballast on the right is greater than the force exerted on the ballast in the middle even though the magnitude of the impact force on the left rail (nearer to the middle of the sleeper) above the sleeper number 80 is higher. In addition, the magnitude of the initial force exerted on the ballast is also different along the turnout due to the variation of the sleeper masses along the turnout. The variation of the sleeper masses will also have effect towards the dynamic of the track in general. This is especially crucial if the condition under the track is of interest such as track settlement prediction. It is because the mass of the sleeper might affect the magnitude of the dynamic vertical force exerted on the ballast and eventually affect the accuracy of the track settlement prediction especially in the switch and crossing panels where the dynamic effect is significant.

Figure 12 shows the maximum force exerted on the ballast along the turnout. The maximum force exerted on the ballast on the left, middle and right started at around the same magnitude 30kN. Due to the formation of the turnout as mentioned earlier, the maximum force exerted on the ballast on the right increases gradually and vice versa for the left. However, the maximum force exerted on the ballast in the middle does not fluctuate as much as the left and the right. Coincidently, at the sleeper number 13, the maximum force exerted on the ballast for all three points are very similar because of the balance of curvature and turnout formation effect. In addition, due to the change of the sleeper geometry back to the ordinary geometry started from sleeper number 93, a reversal effect of the left and the right maximum force exerted on the ballast due to the carbody roll can also be observed.

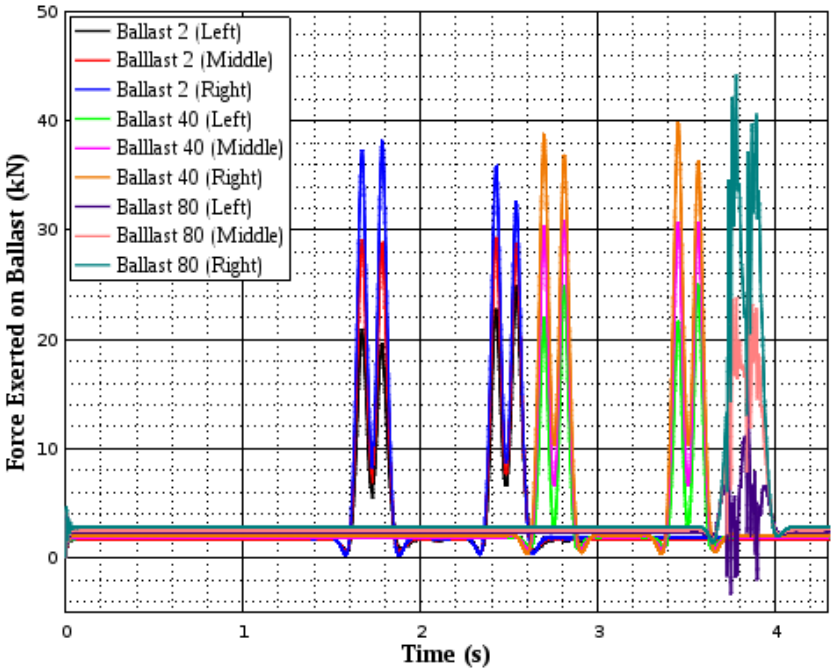

Figure 11: Force exerted on the ballast

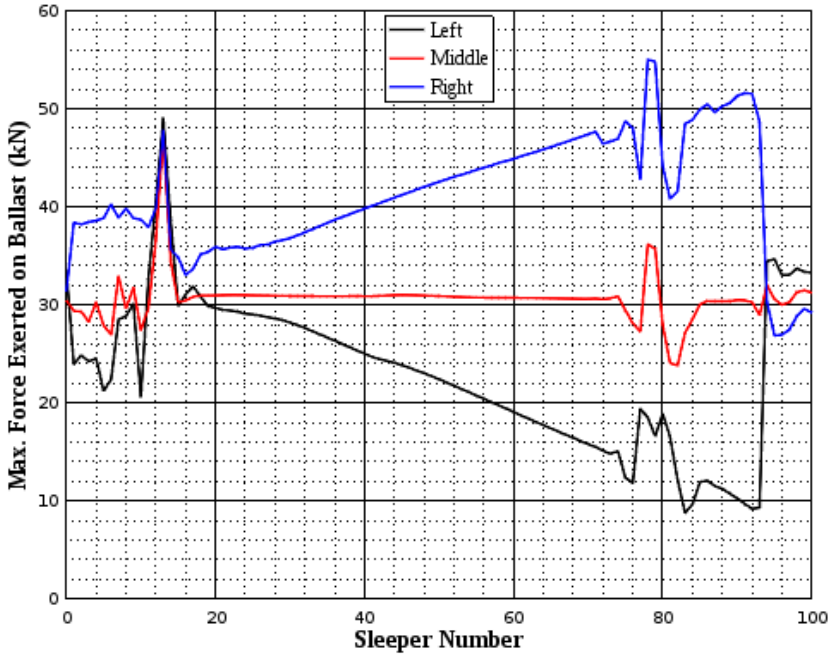

Figure 12: Maximum force exerted on the ballast

As a comparison, the force exerted on the sleeper and the ballast of the leading wheelset for moving mass turnout model is also plotted, see figure 13. It can be seen that the time history for the vertical normal force, the force exerted on the sleeper and the force exerted on the ballast are very similar. This because the vertical normal force transmitted down to the sleeper and to the ground without affecting by the rail bending stiffness, discretisation of the track and the formation of the turnout. The forces exerted on the ballast have a slightly higher magnitude compare to the forces exerted on the sleeper due to the existence of the sleeper mass. However, this variation is constant throughout the turnout due to the consistency of the sleeper mass in the moving mass model.

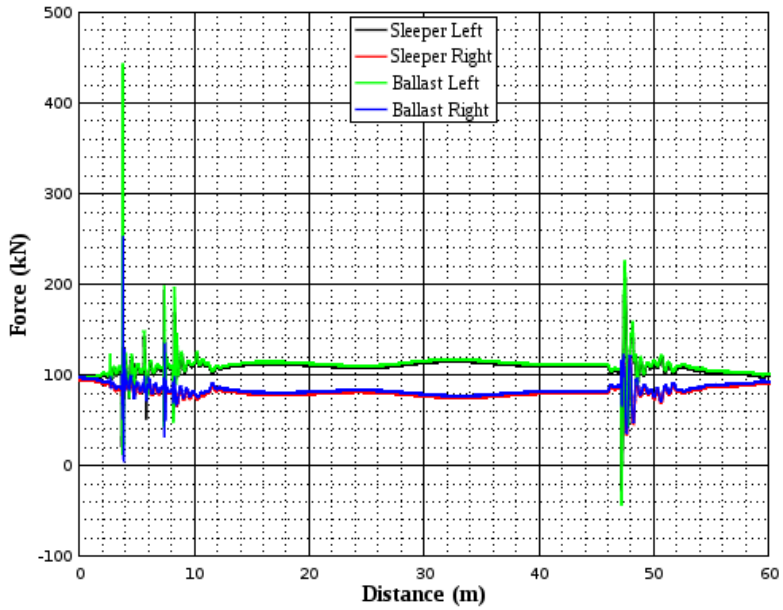

Figure 13: Force exerted on the sleeper and the ballast (moving mass turnout model)

6. Discussion

In most of the cases, railway track is not the major focus in MBS train-track dynamic analysis. This is because MBS tools dedicated for train-track dynamic analysis are mainly used for the train dynamic analysis and the dynamics contributed by the track is relatively low assuming that the track geometry is more or less consistent such as tangent and curve tracks. However, when a more sophisticated track structure such as switch and crossing is involved, the track effects such as rail bending stiffness

and sleeper mass become crucial in order to simulate both train and track dynamics more accurately. The advantages of modelling railway track in MBS using this approach are listed as below:

1. Train and track models can be modelled as a whole.
2. Rail bending stiffness can be modelled and varied.
3. Sleeper mass and track stiffness can be varied.
4. Sleeper passing effect can be modelled.
5. Dynamic interaction within the track can be computed and observed.

In addition, modelling railway track in MBS can make other type of analysis in the track i.e. settlement analysis, inclusion of ballast characteristic, hanging sleeper effect, track geometry irregularity, track components optimisation, etc. possible without over simplifying the train or the track.

The downside of this approach is that generally in MBS, the initiation time increases with the increase of number of bodies in the simulation. For a switch and crossing model, many additional bodies are needed, for example, in this paper additional 400 rail and 200 sleeper masses are needed alongside with the seven bodies for the train model. The initiation of the train-track model took 15 minutes and the simulation took 11 minutes for a computer with processor Intel® Core™ i7-4600 CPU @ 2.10GHz (4CPUs) compared to the moving mass turnout model which took 3 minutes in total to simulate.

For that, a separate algorithm has been written to avoid the repetitive initiation process in which the initiation of the train-track model is saved during the first simulation, so that for the subsequent simulation using the same train-track model, the initiation of the model can be avoided.

7. Conclusion

In this paper, a train-turnout coupled dynamics has been simulated using a multibody simulation software GENSYS. Track parameters such as rail bending stiffness, rail bending stiffness variation and sleeper mass variation along the turnout are considered in the model. The dynamic track properties of the turnout model such as rail masses pitch inertia, railpad stiffness and damping and ballast stiffness and damping are validated beforehand by comparing the receptance functions from a straight track model to the receptance functions recorded in the literature.

After that, the results of the train-turnout coupled model are compared to the results of a moving mass train-turnout model. The following conclusions are drawn:

1. The vertical and lateral normal forces for the train-turnout coupled model is in good agreement with moving mass train-turnout model.
2. The full turnout model has influence towards the vertical and lateral normal forces especially in the switch panel and crossing panel where the dynamic impact is higher.
3. The force exerted on the sleepers of the train-turnout coupled model is lower compared to the moving mass track model because of the rail bending stiffness. Besides, the magnitude of the force exerted on the sleepers decreases with the increase of the rail bending stiffness.
4. The force exerted on the ballast is position of the trainload dependent. For example, in the present paper, the force on the right side of the sleepers are greater along the turnout as the train is travelling through the diverging direction.
5. The time history of the individual track component in the train-track coupled model can be analysed but not the moving mass track model.

It is also concluded that such approach can potentially provide a better train-track interaction result compared to moving mass track model because of the consideration of the track parameters. The future work is to validate the train-turnout model with a real turnout model by receptance test or comparing the components i.e. sleeper or rail accelerations from the real turnout with the numerical model.

Competing interests

The authors of this paper declared that there is no conflict of interests in their submitted paper.

Acknowledgments

The present work was carried out at the Department of Civil and Environmental engineering, Norwegian University of Science and Technology and is funded by The Norwegian Rail Directorate. Mr. Ingemar Persson is also gratefully acknowledged for assisting and advising modelling in GENSYS.

References

[1] C. Alves , A. Paixão, E. Fortunato, and R. Calçada, "Under sleeper pads in transition zones at railway underpasses: numerical modelling and experimental validation," *Structure and Infrastructure Engineering*, vol. 11, no. 11, pp. 1432-1449, 2015.

[2] M. Wiest, E. Kassa, W. Daves, J. C. O. Nielsen, and H. Ossberger, "Assessment of methods for calculating contact pressure in wheel-rail/switch contact," *Wear*, vol. 265, no. 9–10, pp. 1439-1445, 2008.

[3] A. Johansson, B. Pålsson, M. Ekh, J. C. O. Nielsen, M. Ander, J. Brouzoulis, and E. Kassa, "Simulation of wheel–rail contact and damage in switches & crossings," *Wear*, vol. 271, no. 1–2, pp. 472-481, 2011.

[4] A. Paixão, E. Fortunato, and R. Calçada, "A numerical study on the influence of backfill settlements in the train/track interaction at transition zones to railway bridges," *Proceedings of the Institution of Mechanical Engineers, Part F: Journal of Rail and Rapid Transit*, vol. 230, no. 3, pp. 866-878, 2015.

[5] H. Wang, V. Markine, and I. Shevtsov, "The analysis of degradation mechanism in track transition zones using 3d finite element model," *Proceedings of the Second International Conference on Railway Technology: Research, Development and Maintenance*, Civil-Comp Press, Stirlingshire, UK, 2014.

[6] E. Kassa, and J. C. O. Nielsen, "Dynamic interaction between train and railway turnout: full-scale field test and validation of simulation models," *Vehicle System Dynamics*, vol. 46, no. S1, pp. 521-534, 2008.

[7] R. Lagos, A. Alonso, J. Vinolas, and X. Pérez, "Rail vehicle passing through a turnout: analysis of different turnout designs and wheel profiles," *Proceedings of the Institution of Mechanical Engineers, Part F: Journal of Rail and Rapid Transit*, vol. 226, no. 6, pp. 587-602, 2012.

[8] C. Wan, V. L. Markine, and I. Y. Shevtsov, "Improvement of vehicle–turnout interaction by optimising the shape of crossing nose," *Vehicle System Dynamics*, vol. 52, no. 11, pp. 1517-1540, 2014.

[9] B. Pålsson, "Design optimisation of switch rails in railway turnouts," *Vehicle System Dynamics*, vol. 51, no. 10, pp. 1619-1639, 2013.

[10] A. Lau, and E. Kassa, "Simulation of vehicle-track interaction in small radius curves and switches and crossings," *Proceedings of The Third International Conference on Railway Technology: Research, Development and Maintenance*, Civil-Comp Press, Stirlingshire, UK, 2014.

[11] C. Esveld, "Modern railway track," 2001.

[12] J. Evans, and M. Berg, "Challenges in simulation of rail vehicle dynamics," *Vehicle System Dynamics*, vol. 47, no. 8, pp. 1023-1048, 2009.

[13] W. Zhai, and Z. Cai, "Dynamic interaction between a lumped mass vehicle and a discretely supported continuous rail track," *Computers & Structures*, vol. 63, no. 5, pp. 987-997, 1997.

[14] K. L. Knothe, and S. L. Grassie, "Modelling of Railway Track and Vehicle/Track Interaction at High Frequencies," *Vehicle System Dynamics*, vol. 22, no. 3-4, pp. 209-262, 1993.

[15] G. Diana, F. Cheli, S. Bruni, and A. Collina, "Dynamic Interaction between Rail Vehicles and Track for High Speed Train," *Vehicle System Dynamics*, vol. 24, no. S1, pp. 15-30, 1995.

[16] N. Ottosen, and H. Petersson, "Introduction to the finite element method,"*Prentice-Hall*, 1992. Print.

[17] Y. Sun, C. Cole, M. Spiryagin, and M. Dhanasekar, "Vertical dynamic interaction of trains and rail steel bridges," *Electronic Journal of Structural Engineering*, vol. 13, no. 1, pp. 88-97, 2013.

[18] S. Iwnicki, "Manchester Benchmarks for Rail Vehicle Simulation," *Vehicle System Dynamics*, vol. 30, no. 3-4, pp. 295-313, 1998.

[19] S. Iwnicki, "Handbook of railway vehicle dynamics," *CRC Press,* 2006. Print.

Paper C

'A methodology for switch and crossing optimization'

A. Lau, C. Wan, A. H. Løhren and I. Hoff

Proceeding of the First International Conference on Rail transportation (ICRT), Chengdu China, 2017.

Also accepted for publication in American Society of Civil Engineers (ASCE)

Is not included due to copyright

Paper D

'Numerical switch and crossing railpad vertical stiffness optimization'

A. Lau, C. Wan, A. H. Løhren and I. Hoff

Numerical Switch and Crossing Railpad Vertical Stiffness Optimization

Albert Lau[1*], Chang Wan[1], Alf Helge Løhren[2] and Inge Hoff[1]
[1.] *Department of Civil and Transport Engineering, Norwegian University of Science and Technology, Trondheim 7491, Norway*
[2.] *Bane NOR (Norwegian National Rail Administration), Trondheim 7435, Norway*

**Corresponding author email: albert.lau@ntnu.no*

Abstract

Railpad has been proved to be able to help to improve the performance of the railway tracks. However, for track component like switch and crossing (S&C) or turnout with different rail bending stiffness, railpad with homogenous vertical stiffness is yet to achieve its optimal performance. In this paper, railpads vertical stiffness of a right hand turn 60E1-R760-1:15 turnout has been numerically optimized non-homogenously using genetic algorithm (GA). The is modelled in the multibody simulation software GENSYS with two types of trains, passenger train and freight train, traveling through both facing and diverging routes under three different track stiffness: soft, medium and stiff. Railpad vertical stiffness under different conditions has been suggested by the optimization. It is concluded that in general, the softer the vertical stiffness of the railpads, the better the performance of the turnout as long as vertical compressive displacement of the railpad does not exceed 2 mm. In the case of the turnout's railpads have to be installed homogenously, it is safe to use railpad with vertical stiffness not less than 33 MN/m regardless of the stiffness of the track as long as the axle load of the train does not exceed 22.5 ton and is running below 200km/h.

1. Introduction

Switch and crossing (S&C) or turnout is a mechanical component that provides flexibility for railway trains to switch from one track to another. Switchblade in switch panel can be moved laterally into one of two positions to lead the train into facing route or diverging route. Whereas crossing is a component that distinguishes the through and diverging route.

However, such flexibility requires certain degree of geometry changes and discontinuities in both the switch and the crossing panels. Because of the geometry

changes and the discontinuities, high impact forces can often be observed. The high impact forces are also the main contributor to damages to turnout. Based on the database in Bane NOR (Norwegian National Rail Administration), there are around 3548 turnouts in 4475 km Norwegian railway network, or approximately 3.1% of the total length of the Norwegian railway network. However, in 2015, approximately 35% of the entire cost of maintenance of the superstructure were spent on switch and crossing related faults [1]. In addition, 55% of the faults recorded in 2015 were switch and crossing related [2].

As a result, turnout optimization related topics have been very popular in the recently years. Some of the optimization examples are optimizing geometry of the crossing nose [3, 4, 5, 6], switch rail geometry [7, 8], track gauge in switch panel [9], vertical elasticity of crossing panel [10], etc. Later research by Fermér and Nielsen [11] shows that railpad stiffness has great influence towards dynamic contact forces. Railpad elasticity has also been proved to be able to reduce, although not always, rail impact forces, forces on sleepers and forces on ballast which subsequently able to help to combat rolling contact fatigue (RCF) damage in a crossing nose [12]. Most importantly, replacement of railpad can be done easily in a new or in an existing turnout.

Traditionally railpad stiffness is kept homogenously along turnout. However, due to the nature of turnout such as difference in rail bending stiffness and geometry variation, homogenous stiffness is yet to achieve its optimum performance. Wan et al.[10] utilized numerical modelling tool and an optimization technique to investigate the effect of non-homogenous vertical stiffness along a crossing nose and it is concluded indeed by doing so, a better performance crossing nose can be obtained. However, numerical model used in the work is only a 2D model in a crossing panel of which for a complex component like turnout is not always enough.

Inspired by the work, an extended optimization investigation using genetic algorithm in a full 3D numerical train-track coupled model has been considered using a commercially available multibody simulation software GENSYS[13]. The turnout considered in the numerical model is a 60E1-760-1:15 (nominal rail profile 60E1, curve radius 760m, and turnout angle 1:15) turnout. Different train type and different track stiffness on both facing and diverging routes are considered in the optimisation. The aim of the investigation is to provide a general non-homogenous railpad vertical stiffness guideline for the turnout.

2. Train-track model

The train and the track are both modelled in a commercially available multibody simulation (MBS) software GENSYS.

2.1 Train model

The train model consists of seven bodies i.e. one carbody, two bogies and four wheelsets as illustrated in figure 1.

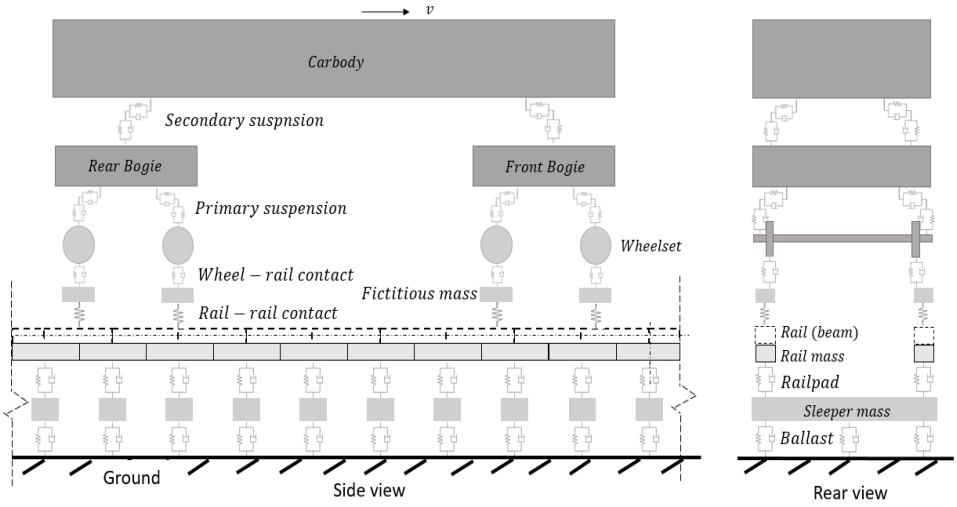

Figure 1: Schematic train-track model

The carbody and the bogies have six degrees of freedom (DOF), namely three translations and three rotations. The wheelsets have five DOFs with the longitudinal displacement being constrained. The bodies are coupled using series of springs and dampers. Two types of trains are used in this study namely passenger train and freight train. The axle load of the passenger train and the freight train is 19 ton and 22.5 ton respectively. The trains have been calibrated with the ones provided by the manufacturers, with good match on eigenvalues and eigenmodes of the vehicles.

2.2 Track model

The turnout model used in this study is a right-hand turn 60E1-R760-1:15 tun without rail inclination. Variation of rail geometry of the turnout is accounted for by applying 30 different rail profiles along the track, see figure 2. Depending on the moving direction of the train, the rail profiles are placed differently. For example, the variation of the rail profiles for diverging move are on the left side of the rail but for facing move, the variation of the rail profiles are on the right side of the rail.

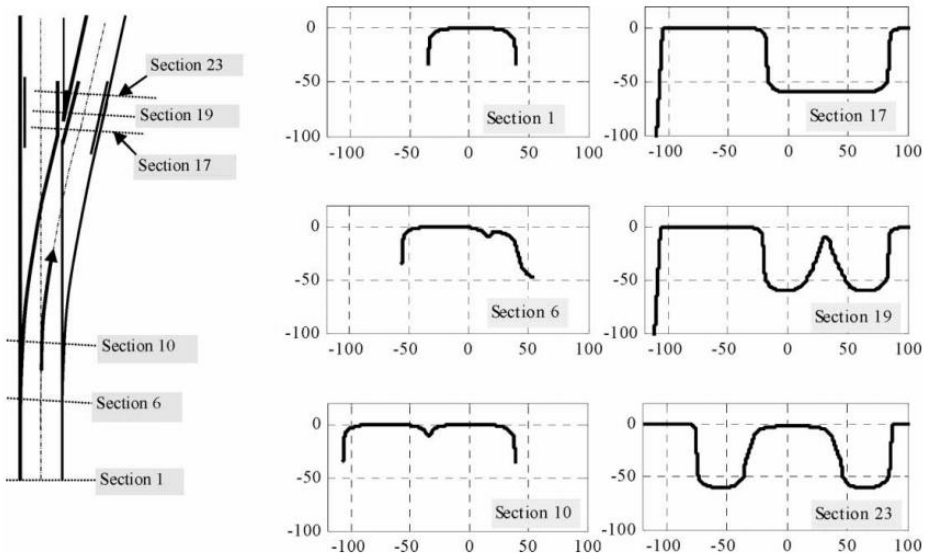

Figure 2: Example of sampling locations and cross-sections of the left rail (diverging move)[14].

The total length of the track model is 120 m, with 60 m of straight track modelled to damp the initial transient effect, followed by 60 m of the turnout. The sleeper span of the track model is set as 0.6 m. The rails are modelled by beam elements with the element equal to sleeper span, so the track model consists of 400 rail masses, 200 sleeper masses and 1000 spring-damper elements (railpads and ballast of the track).

Unlike normal track, bending stiffness of the rails are varied in the turnout. To account for this variation, the rail bending stiffness is defined element-wise along the turnout according to the actual cross-sectional property of the rail. The bending stiffness of the elements is approximated by linear interpolation of the bending stiffness of the two closest adjacent rail profiles. In addition, sleeper properties such as mass, dimension and moment of inertias are also varied along according to the real turnout design.

2.3 Train-track coupling

For coupling of the train and the turnout, a stiff series of spring and damper (k=141MN/m, c= 30kNs/m) is used under each wheel connect to a neglected inertia fictitious mass. The fictitious masses are required in order to extract wheel-rail profile contact information and track irregularity (if any) during the time simulation. The contact information is pre-calculated and save in an offline lookuptable. The fictitious mass is then connected to rail (beam element) by a stiff 'rail-rail' contact stiffness which has a value of 5000 MN/m assuming the wheel and the rail do not lose contact

during simulation. For normal wheel-rail contact problem, Hertz contact theory is adopted. Creepages and creep forces are solved by using the FASTSIM algorithm.

3. Optimization

3.1 Design variable

The design variables in this study are vertical stiffness of railpads. Recent investigations[10, 15] show that adapting non-homogenous stiffness along turnout can yield a better train-track dynamic interaction. However, varying vertical stiffness of the railpad on each individual sleeper might be impractical.

Therefore, to avoid the mistake, only four different zones are defined in this study based on panel definition as shown in figure 2. However, two different zones are considered instead of one in the crossing panel because the rail in crossing nose in the crossing panel and the rail in opposite side of the crossing nose have large variation in terms of rail bending stiffness. This has major effect on both wheel-rail forces and force transferring down to the sleepers.

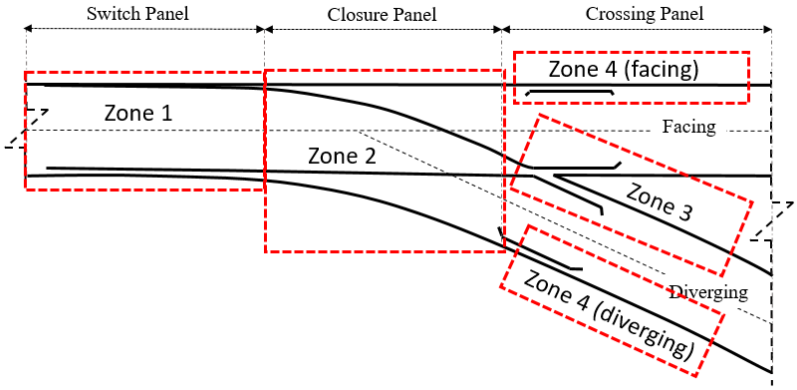

Figure 3: Zone definition

Note that in general, there is a correlation between stiffness and damping properties, such as the classic Rayleigh damping. In this study, however, the correlation between the stiffness and the damping properties is ignored. For example, the damping properties in the vertical direction of the railpad is fixed while the stiffness properties is to be adjusted during the optimization. The design variables are written as a vector with four elements representing railpad vertical stiffness in each individual zone.

$$\boldsymbol{x} = [x_1, x_2, x_3, x_4]^T \tag{1}$$

Subjected to

$$A_i \leq x_i \leq B_i, \qquad i = 1, \dots 4 \tag{2}$$

Where, A_i and B_i are side limits which define lower and upper bounds of the design variables. The lower and upper bounds of the vertical stiffness of the railpad are set to be 10 MN/m and 300 MN/m respectively. The values are chose based on previous studies[15, 16]which showed that the railpad vertical stiffness can be as low as 10 MN/m without violating limits and it does not have much benefit having stiffness higher than 300MN/m.

3.2 Objective function

The objective of the optimization is to minimize maximum vertical wheel-rail force and maximum force exerted on the sleepers. This is because these two forces are often associated with the source of damages to the switches and crossings. Both the maximum wheel-rail contact force and the maximum force on the sleepers are to be reduced in each of the four zones. Therefore, an eight-objective optimization task has to be considered in each optimization problem. For the sake of simplicity, the multi-objective optimization problem is further simplified by formulating the problem as a single objective function using a combined weighted sum.

$$F(\boldsymbol{x}) = \sum_{n=1}^{4} w\left(\frac{F1}{F1^r}\right)_n + w\left(\frac{F2}{F2^r}\right)_n \rightarrow min \tag{3}$$

Where $F1$ is the maximum vertical wheel-rail force, $F2$ is the maximum force exerted on the sleepers, subscript n is zone number, superscript r in the denominators denotes reference of the forces and w is weighting factor. The weighting factor (w = 0.125) is applied for all the eight objectives, assuming that all of them are equally important.

3.3 Constraint

A constraint with respect to potential feasible design has been chosen in this study, namely vertical compressive deflection of the railpad, see table 1.

Table 1: Constraints

Constraint	Value
Maximum allowable vertical compressive displacement of the railpads (mm)	2

Limiting value of 2 mm for the maximum vertical compressive displacement of the railpads is considered. This is to avoid excessive deflection which might lead to event like flange climbing derailment. Other than ensuring potential feasible design of the optimization, the constraint also help to ensure safety and stability of the train-track system. In case of any violation of the constraint, a penalty value will be assigned to the objective value.

$$F_p(\boldsymbol{x}) = F(\boldsymbol{x}) + \sum_{j=1}^{m} C_j \left(\frac{\emptyset}{\emptyset_{allow}}\right)_j^2 (\boldsymbol{x}) \tag{4}$$

Where $F_p(\boldsymbol{x})$is the updated penalized objective function, $F(\boldsymbol{x})$ is the unpenalized objective function, C is the penalty coefficient constraint with value of 0.1, m is the number of constraints which in this study is only one, $\emptyset$ is the violated constraint and $\emptyset_{allow}$ is the corresponding allowable value. The concept of the penalty value is that, when one or more constraints is violated, a penalty value, which is calculated based on the violated constraint normalized by its allowable value multiply with the penalty coefficient is added to the objective. As the penalty value is a quadratic function, the value increases exponentially with the magnitude of the violation. Preferably, the penalty value should be kept just above the limit below which infeasible solutions are optimal. This is because if the penalty value is too high or too low, the problem could potentially become either too sensitive or not sensitive at all to the design [17].

3.4 Optimization

Genetic algorithm namely 'ga' function embedded in MATLAB R2017a [18] is used. Genetic algorithm is a non-gradient based evolutionary optimization technique based on a natural selection process that mimics biological evolution. This optimization technique is used because it is robust and has been successfully applied in many other fields. Moreover, for non-linear train-track problem like this study, the chances for the optimization to end up in local minimal is lower. However, the 'ga' in MATLAB does not handle non-linear constraints, thus penalty value method (as explained in section 3.3) has to be formulated separately in the optimization problem. For each optimization setting, 5 generations with population size of 300 and elite number of 5 were considered.

4. Results and discussion

Each train travels through the turnout on both facing and diverging routes with different ballast stiffness as show in table 2. For the facing move, the speed is set as 200 km/h and 120 km/h for the passenger train and the freight train respectively. For

the diverging move, the speed is set as 80 km/h for the both trains. In total, 12 cases have been investigated.

Table 2: Ballast stiffness.

Ballast stiffness	**Value (MN/m)**
Soft	50
Medium	400
Stiff	3000

Table 3 and 4 show the optimized railpads vertical stiffness and its corresponding results for the passenger train and the freight train respectively under different track conditions. For a better visualization, both reference values and optimized values (***italic and bold***) are included in the same tables. The reference railpad stiffness is 150MN/m homogenously throughout the turnout.

Table 3: Results for the passenger train

Track stiffness	**Dir.**	**Zone**	**Railpad stiffness (MN/m)**	**Max. vertical wheel force (kN)**		**Max. sleeper force (kN)**		**Railpad compressive disp. (mm)**	**Obj.**
				Ref.	***Opt.***	Ref.	***Opt.***		
Soft	**Facing**	1	15	104.64	***101.24***	33.19	***28.48***	1.90	0.8906
		2	16	96.68	***96.31***	37.07	***30.56***	1.91	
		3	18	128.00	***124.31***	44.44	***35.65***	1.98	
		4	15	118.26	***110.96***	38.54	***29.57***	1.97	
	Diverging	1	19	176.32	***171.43***	46.27	***36.78***	1.94	0.8773
		2	20	113.72	***113.39***	41.70	***39.02***	1.95	
		3	17	172.54	***139.30***	39.53	***31.95***	1.88	
		4	14	95.20	***89.45***	41.50	***26.56***	1.90	
Medium	**Facing**	1	21	107.22	***107.77***	48.60	***41.28***	1.97	0.9036
		2	21	92.22	***96.24***	55.57	***41.30***	1.97	
		3	18	168.05	***157.22***	43.14	***34.33***	1.91	
		4	27	114.48	***113.93***	57.73	***52.23***	1.93	
	Diverging	1	21	148.80	***176.87***	68.41	***40.72***	1.94	0.7878
		2	23	113.20	***113.40***	57.15	***44.76***	1.95	
		3	16	224.55	***163.88***	48.39	***31.54***	1.97	
		4	15	111.01	***98.15***	59.26	***27.69***	1.85	
Stiff	**Facing**	1	19	105.83	***106.69***	60.24	***36.06***	1.90	0.8357
		2	33	96.14	***96.35***	66.33	***65.84***	1.99	
		3	15	161.22	***148.74***	41.74	***27.99***	1.87	
		4	22	117.50	***109.88***	77.19	***42.88***	1.95	
	Diverging	1	24	139.63	***172.87***	89.13	***44.41***	1.85	0.7245
		2	24	112.91	***113.34***	71.34	***47.03***	1.96	
		3	16	241.80	***166.57***	63.06	***30.96***	1.94	

		4	15	122.59	***99.30***	70.17	***28.52***	1.90	

Table 4: Results for the freight train

Track stiffness	Dir.	zone	Railpad stiffness (MN/m)	Max. vertical wheel force (kN)		Max. sleeper force (kN)		Railpad compressive disp. (mm)	Obj.
				Ref.	*Opt.*	Ref.	*Opt.*		
Soft	Facing	1	17	*118.37*	***117.78***	*36.87*	***33.05***	1.94	0.9140
		2	16	*111.13*	***111.25***	*33.91*	***31.05***	1.94	
		3	18	*150.08*	***141.53***	*44.42*	***35.77***	1.99	
		4	18	*110.54*	***110.42***	*46.16*	***34.92***	1.94	
	Diverging	1	22	*216.21*	***211.16***	*55.63*	***42.24***	1.92	0.7089
		2	23	*136.08*	***136.21***	*47.36*	***45.23***	1.97	
		3	19	*194.36*	***162.57***	*44.47*	***37.74***	1.99	
		4	16	*107.33*	***101.04***	*47.32*	***30.65***	1.92	
Medium	Facing	1	24	*118.61*	***118.16***	*55.70*	***46.68***	1.94	0.9248
		2	22	*111.59*	***111.52***	*51.72*	***41.91***	1.90	
		3	20	*145.25*	***158.19***	*51.70*	***39.67***	1.98	
		4	28	*110.82*	***110.63***	*61.85*	***55.40***	1.98	
	Diverging	1	23	*192.28*	***198.77***	*66.37*	***45.23***	1.97	0.7884
		2	27	*135.76*	***136.08***	*67.68*	***53.74***	1.99	
		3	19	*260.40*	***191.58***	*55.75*	***36.75***	1.93	
		4	17	*122.58*	***111.62***	*65.22*	***31.95***	1.88	
Stiff	Facing	1	21	*118.33*	***121.65***	*68.98*	***41.39***	1.97	0.8700
		2	33	*111.35*	***111.81***	*65.18*	***64.15***	1.94	
		3	19	*143.13*	***156.33***	*54.54*	***34.32***	1.81	
		4	23	*110.46*	***110.81***	*72.73*	***45.04***	1.96	
	Diverging	1	26	*193.51*	***199.44***	*84.92*	***50.55***	1.94	0.7250
		2	28	*135.41*	***136.08***	*85.06*	***57.40***	1.98	
		3	19	*276.09*	***193.68***	*72.53*	***36.21***	1.91	
		4	17	*130.48*	***111.87***	*74.85*	***32.68***	1.92	

Observations from the table 4 and 5:

1. Soft railpad can help to, but not always, reduce the maximum vertical wheel force.
2. Soft railpad can always help to reduce the force exerted on the sleepers and often significantly.
3. Soft railpad is more effective to reduce the force exerted on the sleepers for the track with stiffer substructure compared to the track with softer substructure.

4. Soft railpad is better in reducing high frequency vertical wheel impact force or so called P1 force. For example, the wheel-rail impact force in the crossing panel has been reduced more compared to the switch panel and closure panel.
5. The optimized railpads stiffness for the turnout based on the current train-track model, zone definition and optimization formulation can be found in table 4 and 5. However, these values should be further tested on-site before a definite conclusion can be drawn.
6. For homogenous railpad vertical stiffness throughout a 60EI-R760-1:15 turnout, it might be safe to use railpad with stiffness of 33 MN/m as long as the axle load is less than 22.5 ton and the train does not travel faster than 200km/h.
7. Deterministic parameter of the vertical railpad stiffness optimization is the vertical compressive displacement of the railpad. Thus, it might be enough to consider only heavier rail vehicle such as freight vehicle in a mixed traffic track for railpad vertical stiffness optimization problem.
8. In most cases, slightly stiffer railpad is suggested when freight train is considered.

Figure 4 shows the vertical wheel forces of the freight train along the turnout in the facing direction with stiff track bed before and after the optimization. Significant reduction can be observed in the switch panel and the crossing panel where the impact force is more significant. Although the optimized maximum vertical wheel force is greater in the both panels, the magnitude of the vertical wheel forces in general is lower after the optimization. However, in the closure panel the results are almost identical to the reference values. Similar trend can be observed on the vertical wheel forces when the freight train travelled through the turnout in the diverging direction, see figure 5.

Note that in the both cases, the reduction of the overall magnitude of the vertical wheel force after optimization is more significant on the wheel that do not experience the rail profile variation and the rail bending stiffness variation, i.e. the left wheel for the facing direction and right wheel for the diverging direction. This is probably because the softer railpads have a better effect in terms of vertical wheel impact when the bending stiffness of the rail is lower. This also highlights the importance of dividing crossing panel into two different zones.

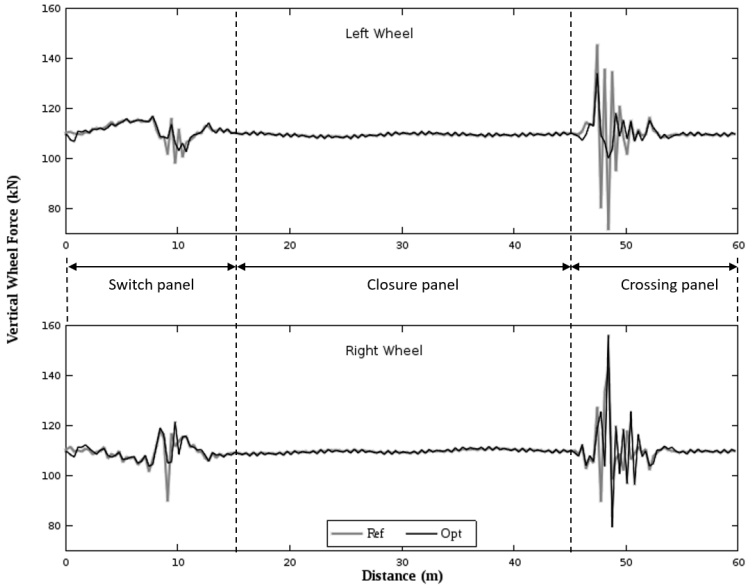

Figure 4: Vertical wheel force in facing direction

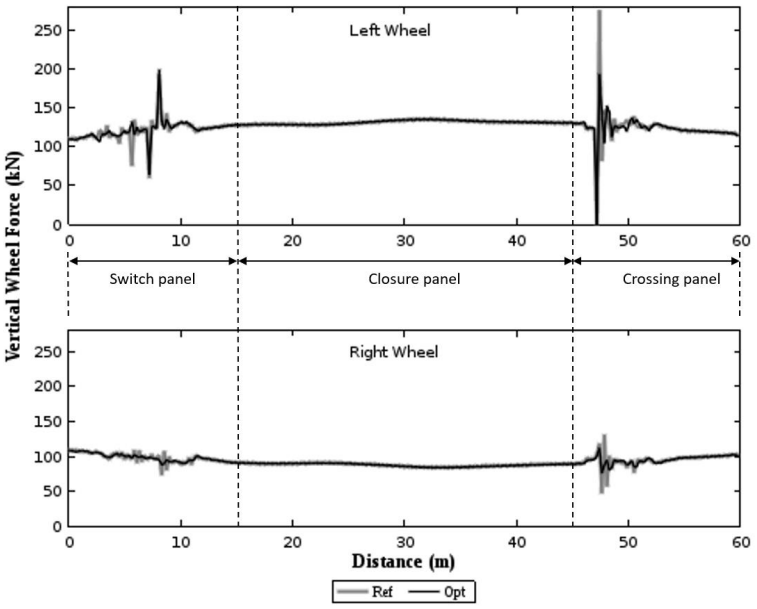

Figure 5: Vertical wheel force in diverging direction.

Figure 6 shows the force exerted the on sleeper 2 (entrance of the switch panel), sleeper 40 (middle of the closure panel) and sleeper 80 (entrance of the crossing panel) when the train travelled though the turnout in the facing direction. The reduction of

the force exerted on the sleeper number 2 is the most significant out of all the three sleepers. This is probably because bending stiffness of the rail allows stiffness of the railpad to be softer and the soft railpad is better in term of force reduction. Due to low bending stiffness of the rail in the closure panel, the wheel force transferring down to the sleepers in this region is slightly higher compared to sleeper number 2 and 80. Therefore, the railpad has to be stiffer in the sleeper number 40 in order not to violate the vertical compressive displacement constraint. This is also the reason the magnitude of the force reduction in the sleeper 40 is lower compared. Although sleeper 80 has the lowest railpad stiffness out of all the sleepers, the magnitude of the force reduction is about the same as sleeper 40 and less than sleeper 2. This is probably because the force exerted on the sleeper is already low due to the high bending stiffness of the crossing nose and the soft railpad can only contribute limitedly to the reduction. Similar trend can be observed for the case when the freight train travelled though the turnout in diverging direction, see figure 7. The reduction in sleeper 40 in diverging route is more significant compared to facing route because the railpad is softer in this case.

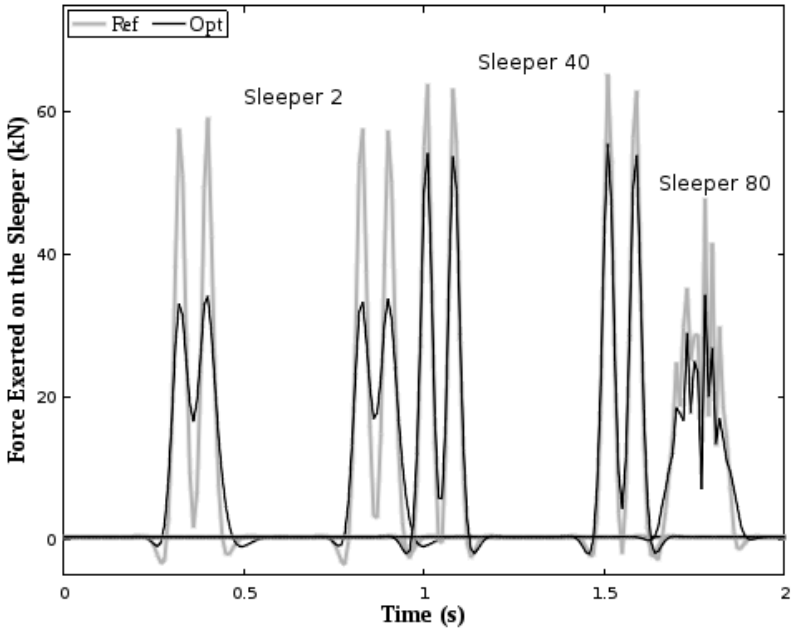

Figure 6: Force exerted on the sleepers under the right rail in facing direction.

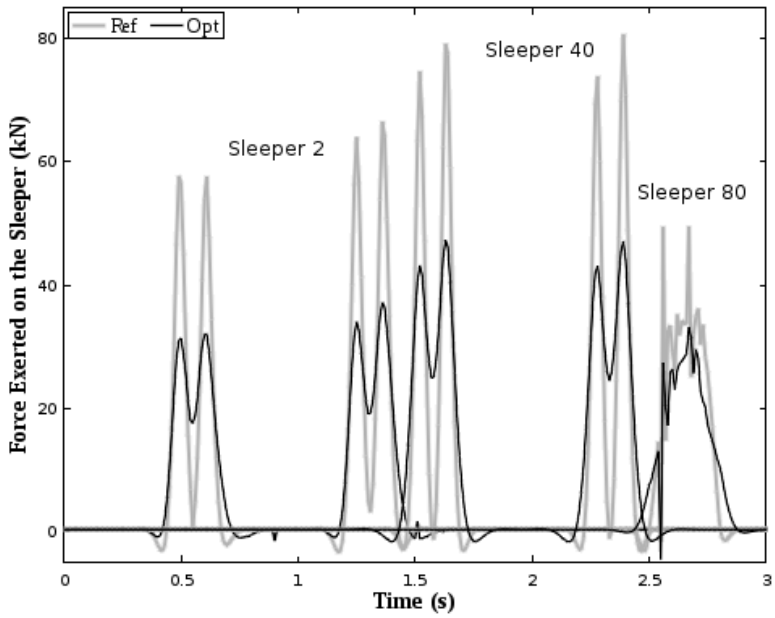

Figure 6: Force exerted on the sleepers under the left rail in diverging direction

One should be cautious when soft railpad is to be used in turnout. This is because soft railpad has direct effect towards gauge widening and may have serious consequences such as flange climbing derailment especially in switch panel and crossing panel. To prevent excessive gauge widening, one can use a special plate pad design with soft middle section but hard side sections as suggested by Ping Wang[16].

5. Conclusion

In this study, railpad vertical stiffness of a standard 60E1-R760-1:15 switch and crossing (S&C) without inclination has been numerically optimized using a train-turnout coupled model coded in a commercially available multibody simulation software GENSYS. To improve performance of the turnout, the railpads stiffness has been considered non-homogenously (zones) along the turnout according to magnitude of the vertical wheel-rail force. Due to the non-homogeneity, the improvement of the turnout is a multi-objectives problem. For the sake of simplicity, the multi-objectives problem is formulated as a single objective function using a combined weighted sum. The nonlinear optimization problem is solved using the genetic algorithm. Different scenarios such as passenger train and freight train running through both facing and diverging directions under three different track

condition i.e. soft, medium and stiff have been investigated and the following conclusions are drawn:

1. Soft railpad vertical stiffness is recommended in order to achieve smaller vertical wheel force and force exerted on the sleepers in the turnout.
2. Soft railpad is able to reduce the force exerted on the sleepers more than the vertical wheel force.
3. In general, the railpads vertical stiffness should be kept as soft as possible as long as it does not violate the defined limit of the vertical compressive displacement.
4. For vertical railpad stiffness optimization, it is probably enough to consider only the heaviest train within the infrastructure travelling with its maximum allowable speed through both facing and diverging directions.
5. It is probably safe to use railpad with stiffness 33MN/m homogenously along the turnout as long as the allowable axle load of the train is less than 22.5 ton and the train is not travelling faster than 200km/h.

The future work from this study is to validate the design and the guidelines on-site. Furthermore to apply the same methodology to other type of turnout design.

Acknowledgement

The work is funded by The Norwegian Railway Directorate (Jernbanedirektoratet).

References

[1] A. H. Løhren, and A. K. Buan. “Utrekk Vedlikeholdskostnader KV overbygning 2015”, Jernbaneverket, Norway, 2015. (In Norwegian)

[2] A. H. Løhren, and K. B. Green. “Feil i Sporveksler 2015”, Jernbaneverket, Norway, 2015. (In Norwegian)

[3] C. Wan, V. L. Markine, and I. Y. Shevtsov, "Improvement of vehicle–turnout interaction by optimising the shape of crossing nose", *Vehicle System Dynamics*, vol. 52, no. 11, pp. 1517-1540, 2014.

[4] C. Wan, V. Markine, and R. Dollevoet, "Robust optimisation of railway crossing geometry", *Vehicle System Dynamics*, vol. 54, no. 5, pp. 617-637, 2016.

[5] B. A. Pålsson, "Optimisation of railway crossing geometry considering a representative set of wheel profiles", *Vehicle System Dynamics*, vol. 53, no. 2, pp. 274-301, 2015.

[6] Z. Ren, S. Sun, and G. Xie, "A method to determine the two-point contact zone and transfer of wheel–rail forces in a turnout," *Vehicle System Dynamics*, vol. 48, no. 10, pp. 1115-1133, 2010.

[7] B. A. Pålsson, "Design optimisation of switch rails in railway turnouts", *Vehicle System Dynamics*, vol. 51, no. 10, pp. 1619-1639, 2013.

[8] P. Wang, X. Ma, J. Wang, J. Xu, and R. Chen, "Optimization of Rail Profiles to Improve Vehicle Running Stability in Switch Panel of High-Speed Railway Turnouts", *Mathematical Problems in Engineering*, vol. 2017, no., pp. 13, 2017.

[9] B. A. Pålsson, and J. C. O. Nielsen, "Track gauge optimisation of railway switches using a genetic algorithm", *Vehicle System Dynamics*, vol. 50, no. sup1, pp. 365-387, 2012.

[10] C. Wan, V. Markine, and I. Shevtsov, "Optimisation of the elastic track properties of turnout crossings", *Proceedings of the Institution of Mechanical Engineers, Part F: Journal of Rail and Rapid Transit*, vol. 230, no. 2, pp. 360-373, 2016.

[11] M. Fermér, and J. C. O. Nielsen, "Vertical Interaction between Train and Track with Soft and Stiff Railpads—Full-Scale Experiments and Theory", *Proceedings of the Institution of Mechanical Engineers, Part F: Journal of Rail and Rapid Transit*, vol. 209, no. 1, pp. 39-47, 1995.

[12] V. Markine, M. Steenbergen, and I. and Shevtsov, "Combatting RCF on switch points by tuning elastic track properties", *Wear*, vol. 271, no. 1–2, pp. 158-167, 2011.

[13] GENSYS user's manual, release 1701. Available from: www.gensys.se.

[14] E. Kassa, C. Andersson, and J. C. O. Nielsen, "Simulation of dynamic interaction between train and railway turnout", *Vehicle System Dynamics*, vol. 44, no. 3, pp. 247-258, 2006.

[15] A. Lau, C. Wan, A. H. Løhren, and I. Hoff, A methodology for switch and crossing optimisation. *The First International Conference on Rail Transportation*, Chengdu, China, 2017.

[16] P. Wang, "Design of high-speed railway turnout: Theory and applications," 2015.

[17] L. Davis, "Genetic Algorithms and Simulated Annealing," 1987.

[18] Mathworks. Global Optimization Toolbox: User's Guide (R2017a)